A COMPREHENSIVE STUDY IN THE APPLICABILITY OF THE SOLID-SOLID STRUCTURAL PHASE TRANSITION OF VANADIUM DIOXIDE TO MICRO-ELECTRO-MECHANICAL DEVICES

by

Rafmag Cabrera

A DISSERTATION

Submitted to
Michigan State University
in partial fulfillment of the requirements
for the degree of

Electrical Engineering - Doctor of Philosophy

2014

ABSTRACT

A COMPREHENSIVE STUDY IN THE APPLICABILITY OF THE SOLID-SOLID STRUCTURAL PHASE TRANSITION OF VANADIUM DIOXIDE TO MICRO-ELECTRO-MECHANICAL DEVICES

by

Rafmag Cabrera

This dissertation presents a series of studies which explores the use of the structural phase transition of VO_2 in MEMS actuators. MEMS actuators enable the interaction of devices with their surroundings, instead of simply sensing it. Actuation mechanisms, which are very common in the macro scale, such as pneumatics, induction motors, and combustion engines, are very difficult and inefficient to implement in the micro scale. Therefore, new actuation techniques must be developed and optimized. Current actuation mechanisms such as electrostatic or thermal expansion have limited performance in terms of total displacement, applied force, operating voltage, and power requirements. This has resulted in a push to incorporate new multifunctional smart materials into standard MEMS devices to improve performance. VO_2 has proven to be one of the most promising materials for the creation of new sensors and actuators. Although most of its electrical and optical properties have been thoroughly studied, there is very little work related to its SPT and its application to MEMS actuators. Throughout this dissertation the SPT of VO_2 is extensively studied, methods are developed for the optimal design of VO_2-based actuators. The memory effect caused by the hysteresis in the SPT is exploited to create very robust programmable multiple state actuators. And fabrication processes are developed which combine the use of VO_2 with standard MEMS fabrication processes.

To my family and friends.

ACKNOWLEDGMENTS

I would like to thank my advisor Dr. Nelson Sepulveda for all the help, guidance and patience he has provided during the years I have known him. He has been a great influence in every step of my professional development. I can confidently say that I would not be where I am, without his help. I would also like to thank all the members of the Applied Materials Group, for their friendship and research collaborations. Im also deeply grateful for the support of Dr. Armando Rua and Dr. Felix Fernandez, who provided me with support through the beginning of my graduate studies.

Im also grateful for the support from the members of my graduate committee; Dr. Tim Hogan, Dr. Shantanu Chakrabartty, and Dr. David Grummon.

I would also like to thank the National Science Foundation for funding my Ph.D through NSF ECCS Award ECCS-1306311 and NSF Award ECCS 1139773 monitored by Anupama Kaul.

Finally I would like to thank my family, without whom none of this would have been possible.

TABLE OF CONTENTS

LIST OF TABLES

LIST OF FIGURES

CHAPTER 1

INTRODUCTION

The insulator to metal transition (IMT) in vanadium dioxide (VO_2) has been studied since 1959 when it was first reported by Morin [11]. VO_2 has proven to be very useful in the creation of new devices due to the fact that many of the materials properties change drastically during the transition (i.e. the material is considered to be a *multifunctional smart material*)[12, 13, 14]. But the characteristic that gives VO_2 the edge over other phase change materials in practical applications, is the fact that the transition temperature is at around 68 ^oC and exhibits temperature hysteresis of several degrees, which can be tuned through doping or choice of substrate. [15]

VO_2 can be deposited in thin films through various methods. All VO_2 films in this dissertation where deposited using pulsed laser deposition (PLD). **Figure** 1.1 shows the electrical and optical characteristic behavior of some VO_2 thin films (deposited by our research group) during the IMT.[16]

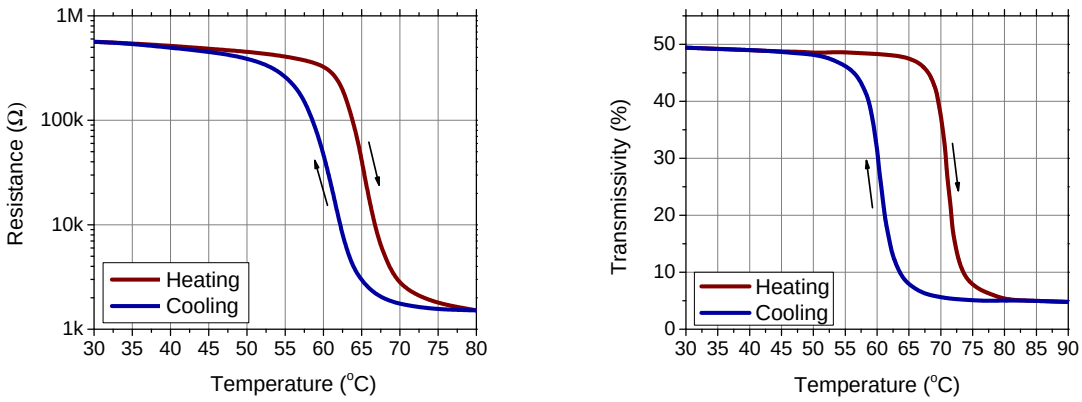

(a) Resistance curve for a VO_2 thin film over SiO_2.

(b) Transmissivity of VO_2 films during the transition.

Figure 1.1 Characteristic behavior of the IMT in VO_2

The crystal structure of VO_2 is tetragonal in its metallic phase. On cooling through

the IMT, this changes to a monoclinic phase by slight reordering of the vanadium ions, which causes a doubling of the unit cell. This change in the structure of the unit cell, hereinafter referred to as the structural phase transition (SPT), can be exploited in the creation of actuators or sensors which, in previous actuator technologies, depended only on the difference in the thermal expansion coefficient between two materials. Because of the very large contraction of the VO_2's crystal plane (during the monoclinic-to-tetragonal change) in the direction parallel to the surface it was deposited on, and the fact that the phase transition of VO_2 occurs over a small temperature variation, the performance of micrometer-sized transducers based on this SPT could provide theoretical limits well beyond the traditionally used mechanisms. More details about this are provided in the second chapter of this thesis.

1.1 Problem Description and Motivation

When a VO_2 film is deposited over a released structure such as a micro-cantilever beam, the resulting changes in film stress during the SPT cause very large deformations in the released structure. These deformations can be exploited to create novel sensors and actuators. In 2010 our research group was the first to report the large deformations achievable in VO_2-based bimorph microcantilevers. Nevertheless, several issues needed to be resolved before VO_2-based actuation technologies became practical. Some of these problems included:

- The need for the characterization of the effects of deposition conditions on the properties of the VO_2 film across its phase change.
- The deformation of released structures with VO_2 films as well as the dynamics of these deformations must be characterized and modeled.
- Different actuation methods need to be studied in order to determine their influence and advantages for different applications.
- Fabrication processes that incorporate VO_2 films must be developed.

This thesis not only addresses this issues, but also explores the difficulties and limitations that come with the integration of VO_2 thin films in MEMS and explores the memory effect in the SPT of VO_2.

1.2 Thesis Statement

This dissertation consists of a series of studies that allow for the development of a fully monolithic MEMS device capable of providing unprecedented capabilities in terms of total actuator displacement. The main contributions of the present work include: the integration of a non-standard MEMS material (VO_2) in well established fabrication technologies; full characterization of VO_2-based MEMS devices by using different actuation mechanisms; development of a fully monolithically integrated device that can exploit the properties of VO_2 to achieve better performance than other available technologies; and the design of a control system that increases the stability and usability of the developed MEMS device in practical applications.

Thesis Statement: *By characterizing and modeling the effects of the structural phase transition of vanadium dioxide when applied to micro-electro-mechanical devices, we intend to significantly expand the capabilities of transducers through the integration of phase-change materials and the development of the necessary tools to cleverly design structures and optimize their performance.*

1.3 Anticipated Research Contributions

This dissertation will directly address each of the research problems listed in **Section 1.1**. A discussion of the deposition conditions and its effects on the SPT of VO_2 will provide a method for optimizing the properties of the VO_2 film for different applications. By characterizing and modeling the deformation of released structures with VO_2 films, it will be

possible to predict the behavior of SPT, thus allowing for the design of VO_2-based devices and simulation of their expected response. By developing and optimizing actuation and detection methods that are compatible with a MEMS fabrication process that includes VO_2, a general architecture that can be used to design future VO_2-based MEMS transducers is enabled. Finally, by incorporating the deposition and patterning of VO_2 films into standard fabrication processes, the design of more complicated MEMS devices is made.

1.4 Dissertation Outline

The remainder of this dissertation is organized as follows; In **Chapter 2** the background information on different MEMS actuating mechanisms, as well as the use of VO_2 and the phase transition, with particular emphasis on the SPT and its effects on the bending caused VO_2 films when deposited over micro-cantilever beams, is discussed in more detail. **Chapter 3** discusses the general memory effect seen in the different properties of the material, and how it can be exploited for different applications.

Up to **Chapter 3** the discussion has only involved simple structures with no built-in actuation method. **Chapter 4** includes a discussion on the design and characterization of a VO_2-coated cantilever beam with built-in micro electric heaters, and their potential use as actuators. The focus of **Chapter 5** is on the application of the memory effect in the SPT, where a close-loop system that compensates for external temperature variations and permits precise control of the programmed states is described. **Chapter 6** presents exploratory studies on possible ways to incorporate VO_2 films into standard fabrication processes. And finally, **Chapter 7**, presents conclusions, and summarizes the contributions of this dissertation.

CHAPTER 2

BACKGROUND

In MEMS, actuators enable the interaction of devices with their surroundings, instead of simply sensing it. Actuation mechanisms, which are very common at the macro scale (i.e. with dimensions in the orders of meters), such as pneumatics, induction motors, and combustion engines are very difficult and inefficient to implement in the micro scale (i.e. with dimensions in the order of 10^{-15} meters). Yet, actuation techniques such as thermal or electrostatic actuation, which are mostly impractical at the macro scale, are ideal at the microscopic level. Micrometer-sized electrostatic actuators use the attractive (or repelling) force between two charged plates or surfaces. Electrostatic actuation has the benefit of a very fast response and low power, but requires very large voltages (100V), and can produce very little force (μN). If lower voltages and higher forces are required, the best approach is to use a thermal-based actuation mechanisms.

2.1 Thermal Actuation in MEMS

When a material is heated its volume changes, this is known as thermal expansion. In a linear dimension, this can be expressed as:

$$\frac{\Delta L}{L_0} = \alpha \Delta T, \tag{2.1}$$

where L_0 is the original length, ΔL is the change in length, ΔT is the change in temperature, and α is known as the **coefficient of thermal expansion** (CTE). For most materials α is positive. α can also vary with temperature, although it is mostly considered constant in the temperature range of interest in MEMS. But most importantly, α is small. For silicon, a change in temperature of 100 ^oC only produces a 0.03% change in size. This means that for

this mechanism to be useful, the deflection must be amplified in some way. There are three main ways this is accomplished in MEMS:

1. The geometry of the structure and its constraints are chosen so that a small expansion in one direction translates to a large deflection in another. (**Section 2.1.1**)

2. The device is designed in such a way so that the temperature of one part of the structure is different from the other. (**Section 2.1.2**)

3. Materials with different CTEs are employed. (**Section 2.1.3**)

2.1.1 Geometrically constrained devices

One of the most common actuator types in this category is known as the bent-beam actuator [17, 1]. This actuator consists of a clamped-clamped bridge, shaped as a "V" made from a single material. An example of this type of actuator is shown in **Figure** 2.1.

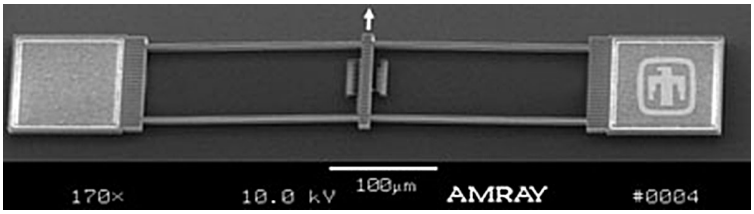

Figure 2.1 Example of an array of bent-beam actuators [1].

The beam is usually heated uniformly by passing a current through it. This will cause joule heating and thermal expansion, which moves the "apex" of the beam. The total amount of force is dependent on the dimension of the beams, the angle of the "V", and the material's mechanical properties. As an example, a 400 μm long, 4 μm wide, and 4 μm thick poly-silicon beam, with an incline gradient of 0.1, has a total displacement of 3 μm when heated 600 ^{o}C. That actuator has a maximum blocked force of 800 μN. That force is about 100 times larger than that of electrostatic comb-drives of similar dimensions [17].

By connecting these beams in parallel, as shown in **Figure** 2.1 it is possible to increase the total force; and by connecting them in cascade as shown in **Figure** 2.2, it is possible to

amplify the total deflection. The structure shown in **Figure** 2.2 has a 4X increase in total deflection.

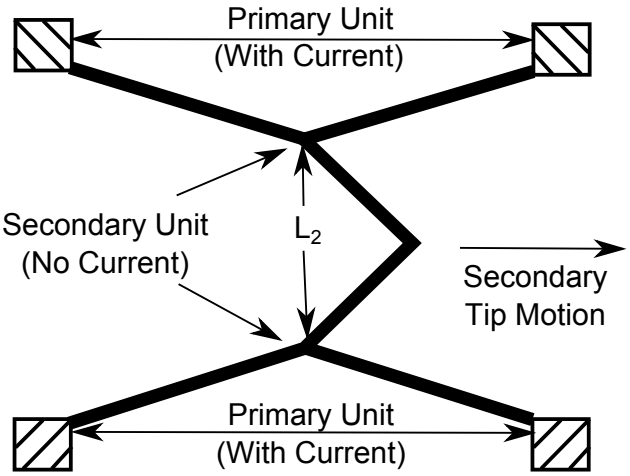

Figure 2.2 Example of a cascade configuration which quadruples the total deflection.

However it is important to note that these results are obtained by heating the devices by 600 ^oC, near the maximum temperature poly-silicon can sustain before self-annealing. This translates to large power consumption (221 mW in the device discussed in [17]). And even in the cascaded configuration the total deflection is less than 20 μm for a total device size in the mm range.

2.1.2 Pseudo bimorphs

If more deflection per size is required with less power consumption, another solution is to use pseudo bimorph structures. In theses structures the thermal and electrical properties of the device are altered in different locations in order to induce a temperature difference between different parts of the structure. This temperature difference will cause one part of the structure to expand more than another, causing bending. One very common geometry is shown in **Figure** 2.3.

In this asymmetrical structure, the width of one "arm" is larger, reducing the total resistance of that arm with respect to the other, and increasing the surface area (which translates into an increase of the heat dissipation in that arm). The end result is that when

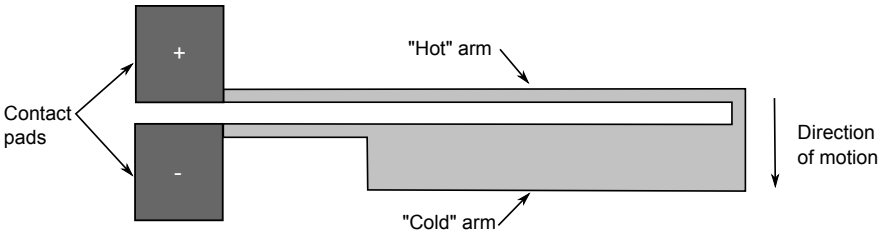

Figure 2.3 An example of a pseudo-bimorph amplification of thermal expansion.

a current is passed through the structure, one arm will heat up (and consequently expand) more than the other. This will cause bending in the direction shown.

This type of device is discussed and tested in [16]. In this work, devices with lengths of 150, 200, 250, 300 μm were tested. For different conditions of "arm" widths, the maximum deflection obtained was 22 μm for the 300 μm device, while dissipating 42 mW of power. This type of thermal device is clearly capable of more deflection per power and size, but the tradeoff is force. The largest blocked force reported for these actuators was 19 μN. Similar to the bent-beam actuators, it is possible to connect these actuators in parallel to increase the total amount force. Because of the small value of the CTE in most materials, it is still necessary to heat these actuators to large temperatures, which still dissipates large amounts of power.

2.1.3 Bimorph Cantilevers

If even more deflection is desired, one approach is to increase the difference in thermal expansion (i.e. increase $\Delta\alpha$), by combining materials with very different CTEs. For example the classical bimorph cantilever (also known as a bi-metalic strip) as seen in **Figure** 2.4.

Here a cantilever beam, composed of two materials with very different CTEs, is heated. One of the layers will expand at a different rate from the other, creating a stress gradient that causes the cantilever beam to bend. It is possible to achieve very large deflections if the proper materials are chosen. For example in [2], a 300 μm long silicon cantilever was coated with a 200 nm thick layer of plasma-polymerized polystyrene (PS). When heated from 20 to 40 ^oC the cantilever beam deflected by almost 50 μm (see **Figure** 2.5)

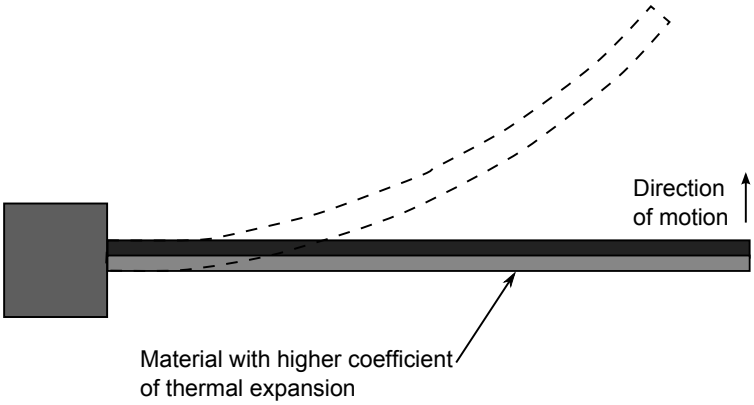

Figure 2.4 An example of a bimorph cantilever.

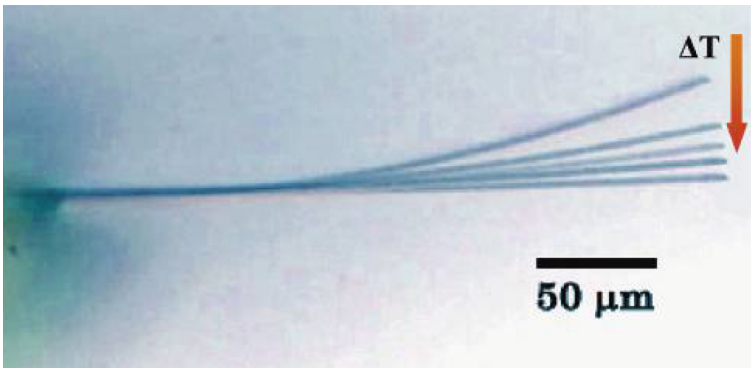

Figure 2.5 bimaterial cantilever bending upon incident heat, side view of the polymer-silicon micro-cantilever bending as temperature increases from 20 to 40 ^{o}C, [2].

This device, is a significant improvement to the other to methods presented in terms of total deflection, since it can produce very large deflections for very small temperature increases. It shows a thermal sensitivity in the order of 1 nm/mK which is 100 times larger than other metal/ceramic bimorph cantilevers and 1000 times larger than the geometrically constrained device discussed in **Section 2.1.1**. However, these types of actuators are made of polymers, which usually have a very low elastic modulus, and therefore their work capacity is limited.

It is possible to create bimorph structures with materials that rely on other physical effects besides thermal expansion. One example is piezoelectric ceramics. In [18], PZT/AgPd bimorph disks with a diameter of 25 mm could produce 75 μm of deflection under an applied voltage of 500 V. However in general piezoelectric materials produce very small deflections

per actuator size and require very large voltages (100s of volts). Therefore their performance can not really be compared to the thermal bimorph structures we are discussing here.

2.2 Phase Change materials

Phase change materials make use of changes in the size of their crystalline structures during a phase transition. The type of materials that are of interest in the use of actuators are usually materials with solid-solid or martensite type transformations. When these materials undergo their phase transition their crystalline structure changes, and with these changes most of the materials properties change as well. Two popular examples of phase change materials are $GeSbTe$ and shape memory alloys (SMA).

2.2.1 GeSbTe

$GeSbTe$ is a phase change material commonly used in re-writable compact discs (CD-RW or DVD-RW). Its crystalline structure can be reversibly changed between amorphous and crystalline states by sequences of heating and rapid cooling. These two phases produce big differences in optical reflectivity [19, 20] and electrical resistivity [21, 22]. But more importanly for MEMS actuator applications, wafer curvature measurements have shown large stresses in the GPa range during the transition [23]. These generated stresses can be used to create a bimorph type actuator. For example in [24], Amorphous $Ge_2Sb_2Te_5$ films were deposited on the SiN cantilevers measuring 50 μm in length. A laser was used to heat the cantilever, this caused a crystallization of the film which caused a change in volume and the cantilever deflected by 8.4 μm. However even though the transition could theoretically be reversed, this requires raising the temperature to the melting point of the film, followed by a rapid cooling usually in the nanosecond range. This rapid cooling is not feasible in micro actuators. This also makes the transition discontinuous, in other words it becomes very difficult to control the deflection of the cantilever at an intermediate value of the transition.

2.2.2 Shape Memory Alloys

Another popular phase change material is SMA (Shape Memory Alloy). SMAs can also undergo a thermally induced crystalline transformation between a low temperature martensitic phase and a high temperature austenitic phase. During the low temperature phase the material is highly ductile and can be easily deformed. When heated the material strength increases and it recovers its initial shape. Ni-Ti based SMA have been shown to recover up to 8% strain or produce up to 500 MPa stress when constrained [25]. Since the SMA transition is "one-way", in other words the material can only return to the high temperature state, some bias element is required to deform the material to the cold temperature state [26, 27]. Currently SMA have the largest strain energy density as will be shown in **Section** 2.4. It was also shown the SMA transition also occurs at the microscopic level [28]. **Figure** 2.6 shows a 3 μm long Ti_5NiCu/PT bimorph cantilever when heated it exhibited a 230 nm deflection [3].

In [3] the Pt film served as the bias element (a form of spring) to restore the cantilever deflection to its cold state. Heating was performed using photo-thermal actuation.

It is important to note that each of these materials brings their own complications when used in MEMS devices. For example, piezoelectric ceramics require extremely large voltages, and although they have the potential to create large forces, they create very small displacements –millimeter size structures are needed to produce 10s of μm deflections. SMAs can produce displacements in the required scale, but their integration in MEMS involves very complicated fabrication processes. Furthermore, the phase transition in SMAs is not fully reversible and starts fatiguing (dependent on the magnitude of the applied stress) after a few hundred cycles [29].

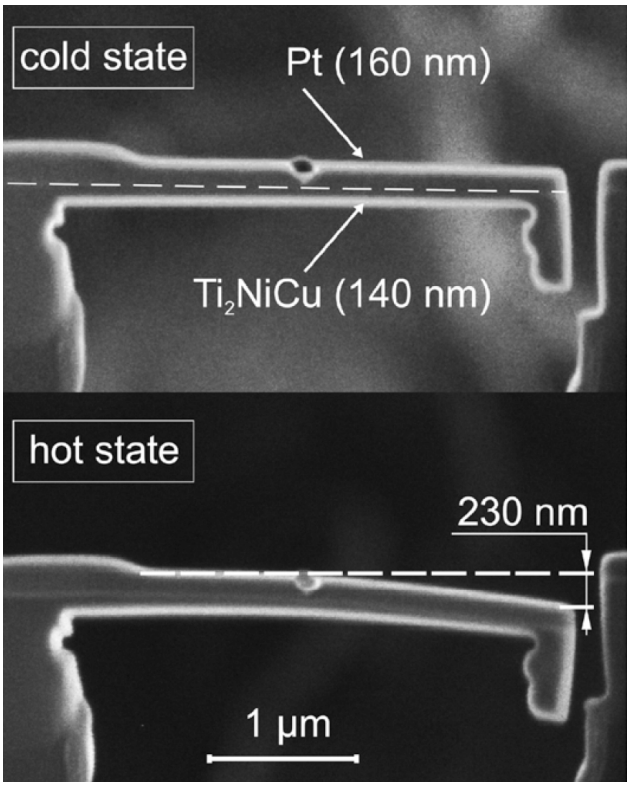

Figure 2.6 0.9 μm^3 working composite shape memory actuator. On thermocycling the actuator exhibits reversible free end deflection of 230 nm, [3].

2.3 The Structural Phase Transition of Vanadium Dioxide

Another phase-change material that has proven to be very useful is VO_2. As was briefly described in **Chapter 1**, VO_2 is a multifunctional material with a transition temperature at around 68 ^oC. The crystal structure of VO_2 is monoclinic (designated M_1), as its temperature rises above 68 ^oC the structure changes to its tetragonal phase,(rutile type, designated R), by slight reordering of the vanadium ions. This is known as a Structural Phase Transition (SPT) **Figure** 2.7 [4]. This SPT is strongly coupled to the IMT in the material. It is important to note that vanadium has 4 stable adjacent oxidation states; VO, V_2O_3, VO_2, and V_2O_5. There are also various other distinct phases of vanadium oxides, for example V_6O_{13}. Some of these oxides also exhibit solid phase transitions, but they either occur at very low temperatures (-123 ^oC for V_6O_{13} [30]), or very high temperatures (280 ^oC for V_2O_5 [31]). The fact that the transition temperature of VO_2 is so close to room temperature, is

what makes the material so useful for transducer applications.

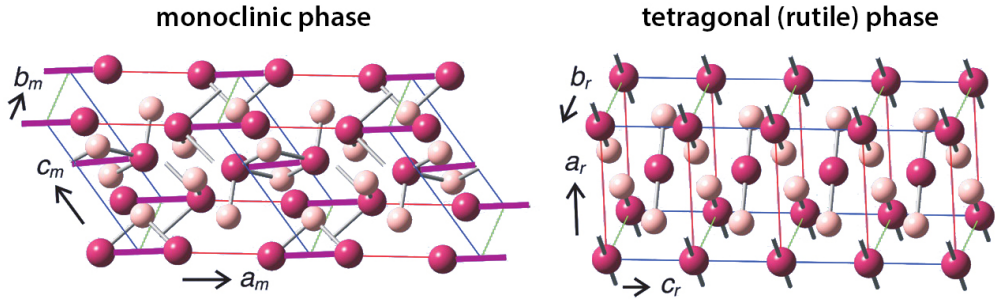

Figure 2.7 Crystal structure of the monoclinic, low-temperature phase (left) and the rutile, high-temperature phase (right). Vanadium atoms are depicted in red and oxygen atoms in a lighter color. Because of a symmetry-breaking pairing of vanadium atoms (violet lines), the axis definitions change [4].

Using the lattice parameters for both phases of VO_2 (and noting that the unit cell in the monoclinic phase corresponds to two unit cells in the tetragonal phase), it can be calculated that the volume of the VO_2 unit cell increases during this SPT. Although the overall volume increases during the phase change (that is, during the heating cycle), the areas of some planes are reduced [32]. When polycrystalline VO_2 films are deposited by pulsed-laser-deposition (PLD) over amorphous SiO_2 or single crystal silicon (SCS), the material tends to orient itself with its (011) and (110) planes parallel to the substrate. The area of the plane for the tetragonal phase is smaller than that of the monoclinic phase. Thus, when SiO_2 or SCS microcantilever structures are coated with VO_2 films, the structure bends concave toward the VO_2 film coating during the phase change. "It can be readily calculated that the area of the plane parallel to the substrate shrinks by 1.7% which results in a theoretical maximum strain of a perfectly oriented and unrestricted film of approximately -0.8%. However, since the film is polycrystalline, and the orientation of every grain is not exactly in the same direction and the film is partially restricted by the substrate, which is precisely what generates the bending, the measured strain was closer to -0.3% [5].

In a preliminary observation [5], the VO_2/Si bimorph cantilevers exhibited very large reversible changes in curvature through the SPT. The superimposed pictures in **Figure** 2.8, for a 350 μm long cantilever, were taken through a low-power microscope as the temperature,

measured with a thermocouple attached directly to the chip, was raised. Cantilever bending toward the side with the deposited film evidences increasing film tension. As the temperature was then reduced, the reverse response was observed, with some noticeable hysteresis.

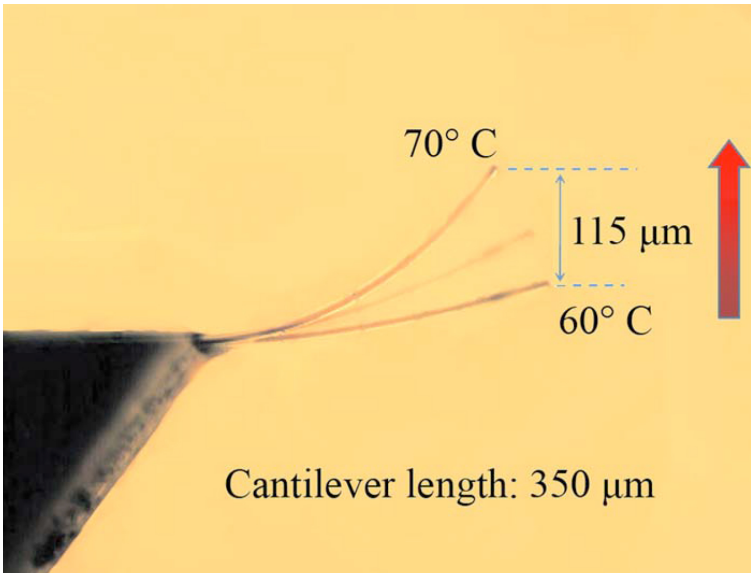

Figure 2.8 Multiple exposure picture of VO_2-coated silicon cantilever during heating [5].

If the amount of deflection per actuator size is compared, VO_2-based actuators can produce twice as much deflection per actuator size compared to the best case polymer/ceramic bimorph actuator. In terms of sensitivity to temperature, VO_2/Si bimorph cantilevers demonstrate an extremely high rate of change in curvature of up to 485 $m^{-1}K^{-1}$ near the transition temperature, which is almost an order of magnitude higher than for the best cases reported for polymer-coated or SMA-coated cantilevers [5].

2.4 Strain Energy Density

Strain energy density is a value that can be used as a figure of merit to compare micro-actuators based on different materials or physical phenomena. It is a value that describes the capability of the actuator to do work, in terms of the actuator size; or, in other words, it normalizes the work that can be generated by the micro device per unit size. in [25], the

Strain Energy Density for different materials was studied. These results are summarized in **Figure** 2.9, together with a VO_2-based microactuator studied in [6].

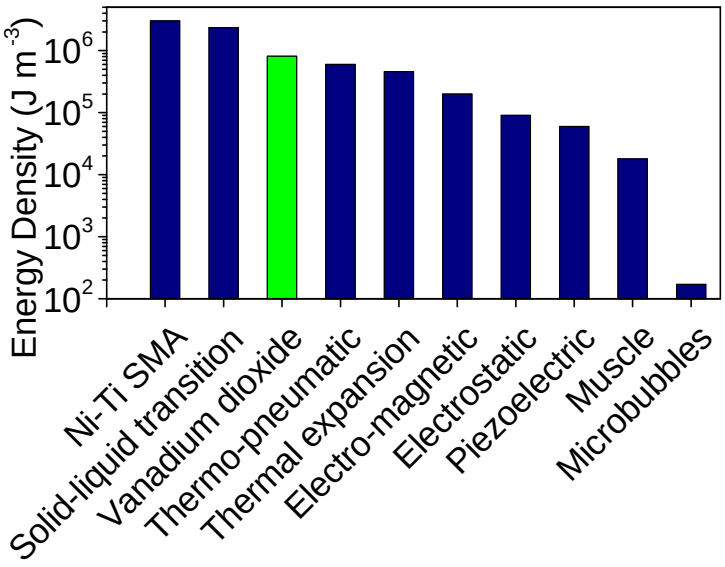

Figure 2.9 Strain energy densities of different micro-actuators including the VO_2-based micro-actuator studied in [6] (green).

Even though VO_2-based actuators do not exhibit the highest energy density, it does posses some advantages over its closest competition. In terms of strain energy density, electroactive polymers have demonstrated strain energy densities of $5 \times 10^4\ J/m^3$, and thermal expansion mechanisms have shown values in the range of $10^5\ J/m^3$. Shape memory alloys (SMAs) have shown the largest strain energy densities ($3 \times 10^6\ J/m^3$) [25], while VO_2-based actuators follow with reported values of $8.1 \times 10^5\ J/m^3$ [6] ($6.3 \times 10^5\ J/m^3$ for initially curved actuators [33]). SMAs are made of ductile metals (typically titanium, nickel, and copper) and are thus more susceptible to plastic deformation, creep, oxidation, and fatigue. In contrast, the bonding in monoclinic VO_2 is ionic, and the compound has little or no ductility. Also, typical SMAs need a wider temperature variation for inducing the phase change, lose their memory capability, and are currently limited to relatively low operating frequencies [33, 25]. Long term studies on the efficiency and fatigue of VO_2-based devices have not been performed, but the actuators discussed in **Chapter 4** of this dissertation have been operated for thousands of cycles at full deflection, without any noticeable evidence of

degradation.

2.5 Summary

This chapter discussed the different actuation mechanisms used in MEMS. Thermal based actuation has proven to be the most practical for large deflection and force. Compared to other forms of actuation, such as electrostatic and piezoelectric, it operates with much lower voltages that are compatible with most electronic devices. The different techniques used to amplify deflection where discussed, of which bimorph structures produced the most deflection per actuator size. Finally, the effects of choosing the right materials in actuators was shown to be critical in the design of efficient bimorph actuators.

Of the many materials that can be used in bimorph structures, VO_2 offers many advantages over current state-of-the-art micro-actuation technologies, as the results in this thesis show. Some of those advantages include high sensitivity, relatively large strain energy densities, and lower power consumption than typical thermal actuators. During the rest of this dissertation the properties and performance of VO_2-based devices will be discussed as well as the possibility of incorporating VO_2 films in MEMS fabrication processes.

CHAPTER 3

THE MEMORY EFFECT IN VANADIUM DIOXIDE

The changes in the properties in VO_2 during its phase transition show hysteretic behavior. This hysteresis allows for the creation of systems with multiple stable outputs for one input. This endows the material with memory capability. Because a similar hysteretic behavior is seen in all of the material properties that change during the transition, different types of memories (e.g. optical, electrical, mechanical) can be created. Furthermore, the intrinsic multi-functionality of this material allows the use of different 'writing mechanisms', the most commonly used being thermal. In this chapter, the memory behavior in the optical, electrical, and mechanical properties of VO_2 is demonstrated.

The experiments described were performed with three different samples coated with VO_2 thin films: 1. a SiO_2 microbridge (used for experiments in which only resistance was measured) 2. a flat SiO_2 glass substrate, used for experiments in which IR optical transmittance was measured, and 3. a single crystal silicon (SCS) microcantilever used for measuring the deflection. The SiO_2 bridge was fabricated by standard lithographic techniques as described in [34] and had length, width, and thickness of 200 μm, 35 μm, and 3.3 μm, respectively. *The work related to this chapter was published in [7, 8].*

3.1 Electrical Memory

The experiments described in this section were performed on the SiO_2 microbridges described before. The microbridges were kept under vacuum (10 mTorr or less) in order to reduce convective heat losses. The back side of the substrates (opposite to the side with the VO_2 thin film coating) was cemented with silver paste to a heater integrated in a sample holder. Thermocouples were directly attached to the samples, and read by temperature controllers feeding the heaters. To allow film resistance readings, gold wires leading to the vacuum

chamber electrical feedthroughs were attached to each of the two bridge anchors, allowing current flow along the bridge.

In order to characterize the hysteresis of the sample, The resistance was measured while employing computer-controlled heating-cooling cycles, were the breadth of the cycles were progressively narrowed. This resulted in the family of curves shown in **Figure** 3.1. These curves can be used to predict the ''path" the resistance will follow given a known temperature variation.

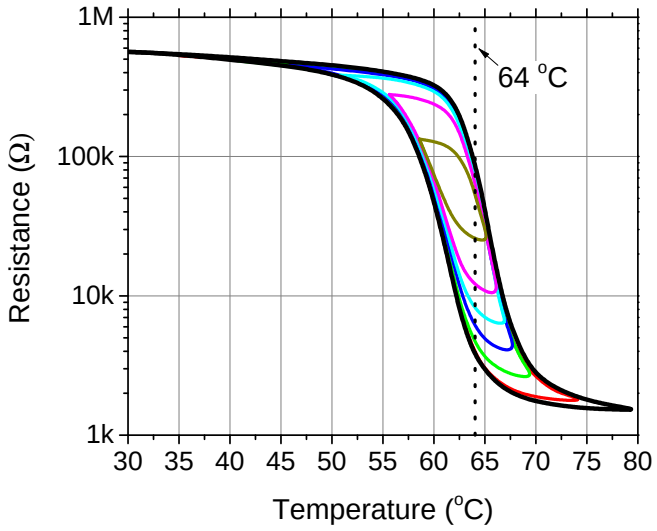

Figure 3.1 Series of hysteresis curves for VO_2-coated microbridge sample. Interior curves are obtained by cooling before the end of the transition region is reached [7].

The memory effect only exists within the hysteresis region of the transition. Therefore, in order to characterize the memory of the film, the sample needs to be kept at a background temperature of 64 ^oC. This was done using the temperature controller. This temperature, about half way through the transition will be reffered to as the "operating temperature". It is important to note that this is the temperature of the sample, which is measured far from the microbridge. Therefore, if the microbridge is locally heated (its localized temperature increases), the rest of the sample will remain at 64 ^oC, and once that temporary source of heat is removed the localized temperature of the microbridge will return to 64 ^oC. The

doted line in **Figure** 3.1 shows that the measured resistance at 64 ^oC can have any value from 95 $k\Omega$ to 4 $k\Omega$ depending on the 'history' of the sample temperature. In other words the same heat input could result in two different values of resistance; depending on what the initial resistance value was (i.e. depending on what was the resistance state prior to the pulse). In this experiment the temporary heat source (actuation method) is the increase in temperature of the sample due to absorbed photons (i.e. photothermal actuation).

In this work, photothermal actuation is achieved through laser pulses. A current-controlled continuous diode laser with 672 nm wavelength and a maximum power output of 300 mW is used to illuminate the samples. The output power was calibrated with an optical power meter (Thorlabs PM100D); and an electronic shutter (Uniblitz T-132) was used to control the duration of the pulses. The laser was focused to illuminate an area of the sample on which the resistance measurements were performed. **Figure** 3.2 shows the change in resistance due to a light pulse irradiating the sample for 2 s, after it was heated from 30 ^oC to 64 ^oC.

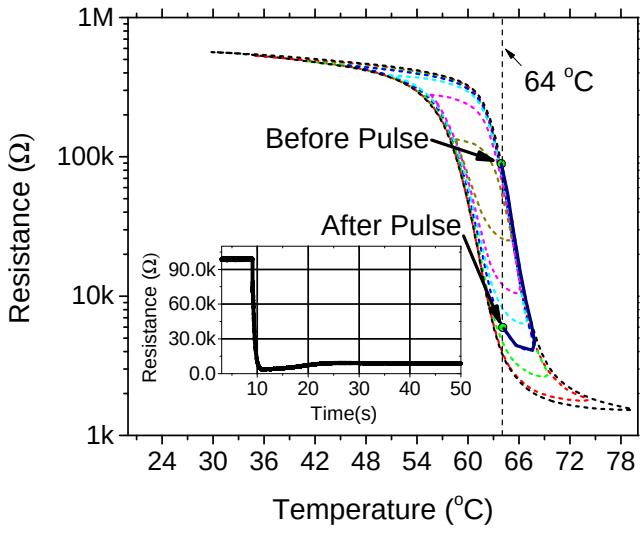

Figure 3.2 Transient of the resistance to a 2 s light pulse. The inset shows the response in the value of resistance when a 2 s red ($\lambda = 672$ nm) light pulse illuminates the sample. The bolder trace in one of the hysteresis curves suggests the thermal evolution of the sample [7].

The resistance drops rapidly while the pulse lasts, then partially recovers more slowly,

but it does not follow the same path during the duration of the pulse. It stabilizes at a value an order of magnitude lower than the initial resistance. The dynamic is suggested by the highlighted hysteresis trace in **Figure** 3.2, which was chosen to connect the initial, lowest, and final resistance values measured before, during, and after the laser pulse, respectively. The behavior shown in **Figure** 3.2 suggests that the final value of the resistance is only dependent on the maximum temperature the sample temporarily reaches. This can be confirmed by adjusting the duration of the light pulses. In **Figure** 3.3, all light pulses had the same intensity as before, but durations were chosen to produce roughly similar resistance drops.

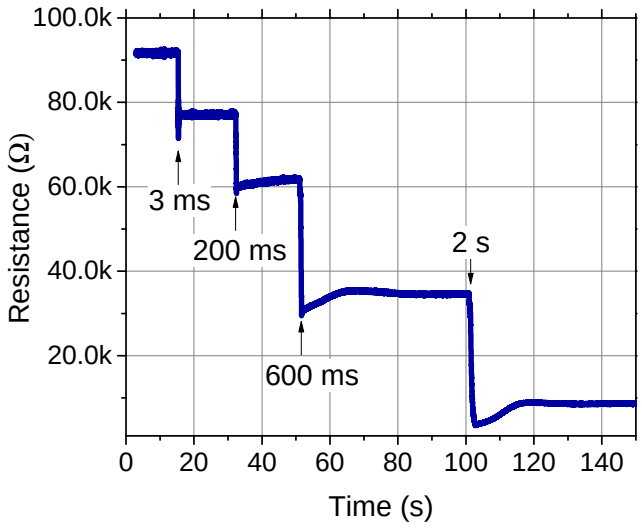

Figure 3.3 Resistance as a function of time as a series of four light pulses with increasing duration illuminate the sample [7].

Starting from the initial condition, as shown in **Figure** 3.3, the magnitude of the drop in resistance increases with the energy of the laser pulse. In this case, the energy of the pulse is increased by increasing its duration. It is noted that the single 2 s pulse (inset **Figure** 3.2) causes nearly the same resistance drop as that due to the cumulative effect of all the pulses recorded in **Figure** 3.3, of which the last pulse is also 2 s long. This suggests that the final resistance value, after the pulse, is not a function of the current value, but only a function

of the largest temperature achieved during the temperature excursion.

3.2 Optical Memory

This experiment was also performed under vacuum (10 mTorr or less) in order to reduce convective heat losses. The sample was cemented first to a thin copper plate with a small (4 mm diameter) circular aperture. This copper plate was cemented in turn to the heater. The light source for the transmittance measurements was a continuous IR laser diode (Mistubishi ML725B8F, 1.31 μm wavelength, 10 mW rated power) with collimating lens, mounted in a thermoelectric cooler base and driven at constant temperature and power by a laser diode driver (Melles-Griot DLD203). A light detector with high IR sensitivity (Thorlabs PDA10CS) was positioned directly opposite. For the transmittance measurements the setup was calibrated with a similar uncoated substrate in place of the sample. The actuation laser system was the same used in **Section 3.1**. Because the area illuminated by the heating laser did not fill the area sampled by the IR laser, this procedure is adequate for measurements of changes in average transmittance in a fixed setup, which is sufficient for the purpose of this work, but would be inadequate for absolute measurements.

The hysteresis curve for sample transmittance at $\lambda = 1.31\mu m$ is shown in **Figure** 3.4. For this particular sample the hysteresis loop is nearly double that of the sample used in **Section 3.1**. Because of the change in the shape of the hysteresis curve a temperature of 70 ^oC was chosen as the "operating temperature".

Figure 3.5 shows the effect of a sequence of pulses with equal irradiance and increasing duration, starting with a 0.6 s pulse and increasing by 0.6 s for each successive pulse. By the end of this sequence, even though the pulse energy continues to increase, the steps become smaller as the value of transmittance approaches the lower limit measured before. As in **Section 3.1**, in which light pulses were used for heating the sample, it was found that approximately the same transmittance reduction can be achived with a succession of many pulses of increasing duration ,that with a single pulse with the same duration as the last

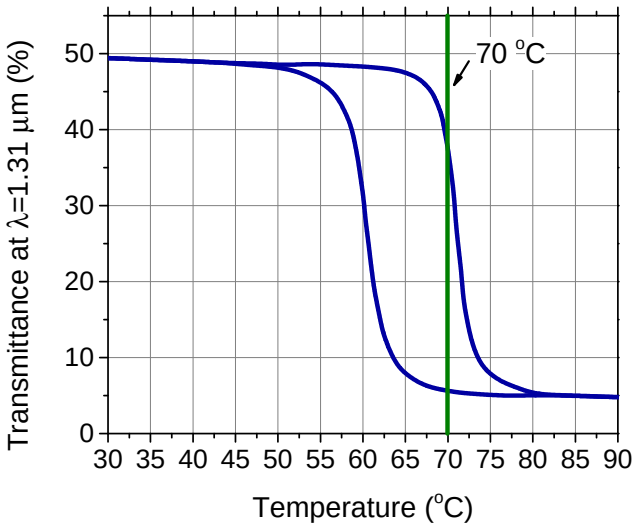

Figure 3.4 Hysteresis curve for transmittance at $\lambda = 1.31\mu m$ for VO_2-coated flat sample [7].

in the sequence, as long as the device is allowed to 'settle' between pulses and the lower transmittance limit has not been reached.

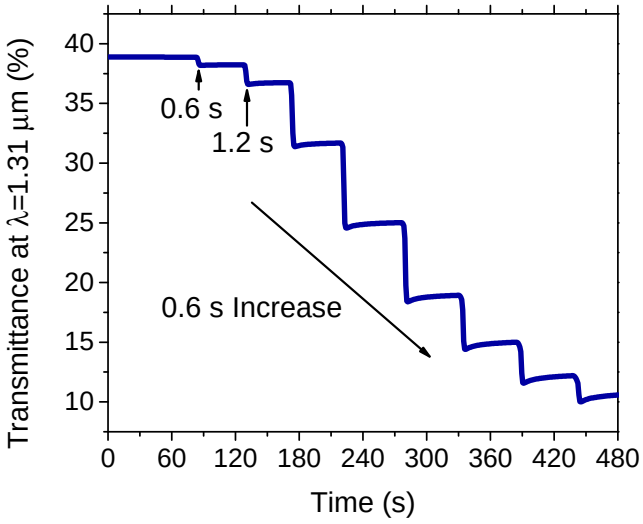

Figure 3.5 Transmittance measured at $\lambda = 1.31\mu m$ for the VO_2-coated flat sample after it was illuminated with a series of red (λ =672 nm) light pulses with equal irradiance and increasing duration, starting with a 0.6 s pulse and increasing by 0.6 s each time [7].

In order to verify the stability of the systems described, the setup for this last case was used to measure the IR transmittance continuously for 8 h, after the sample was brought up

to 70 ^{o}C, subjected to a single light pulse during which transmittance was lowered from 38.5% to 25.0% and maintained at the same temperature. During this time the transmittance value slowly decreased to 24.8% by the time the experiment was ended. This slight reduction was attributed to instrumental drift in the temperature control or IR emission-detection system.

A second experiment was performed with this sample in order to demonstrate the capability to combine the electrical and optical properties of the VO_2 film. Voltage pulses were applied through wires directly connected to the VO_2 film as the transmittance was measured. As shown in **Figure** 3.6, a sequence of pulses with increasing duration but equal voltage (80 V in this case), produces successive drops in sample transmittance. As in the previous case with the resistance measurements, there is some overshoot of the transmittance value just as the pulse ends, associated with thermal excursion in the region excited. The transmittance recovers rapidly, however, and remains at the,new level when the local temperature stabilizes. The second trace in **Figure** 3.6 was obtained by applying pulses of equal duration (1 s) but increasing voltage.

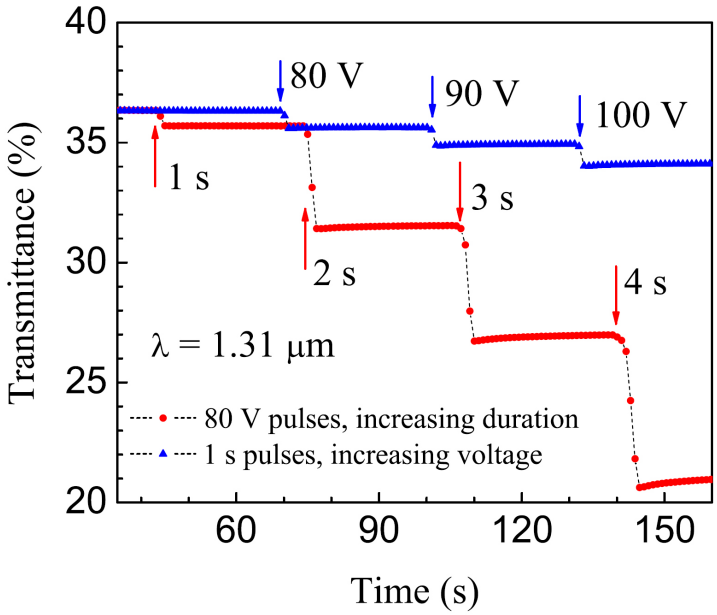

Figure 3.6 Sample transmittance at =1.31 μm for the VO_2-coated flat sample in response to a series of 80 V electric pulses with increasing duration lower curve and to a series of increasing voltages with equal 1 s duration upper curve [7].

3.3 Mechanical Memory

The samples in this section consist of a VO_2 film deposited over commercially available silicon micro cantilever chips (MikroMasch). As specified by the manufacturer, the cantilever used for the detailed measurements had length, width, and thickness of, respectively, 350, 35, and 1 μm, and a spring constant of 0.6 N/m. **Figure** 3.7 shows an SEM image of the cantilever chip.

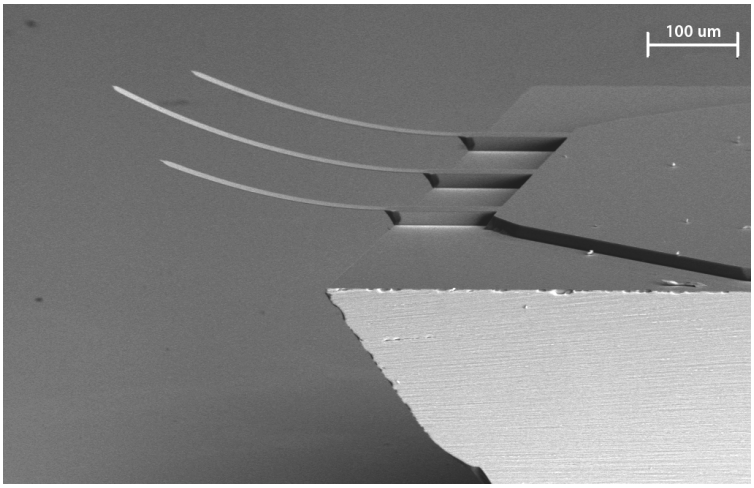

Figure 3.7 SEM image of the commercially available silicon micro cantilever chips (MikroMasch). The center cantilever is 350 μm long.

Figure 3.8 shows a schematic of the experimental set-up used for this experiment. The entire setup is constructed on an optics air-suspended table in order to reduce vibrations. In this setup, a red laser (L1; $\lambda = 672$ nm, intensity = 500 μW, spot size 35 μm), was focused and aimed at the tip of the VO_2-coated Si cantilever. This laser was used to measure the deflection of the cantilever beams, and remained on during the experiment. The reflected beam is then aimed at a position sensitive detector (PSD) (Hamamatsu S3270). As the cantilever moves the PSD will produce a voltage proportional to the displacement, using the initial position of the cantilever as a reference. The second laser (L2; $\lambda = 672$ nm, spot size 100 μm) was centered at 100 μm from the cantilevers anchor. This laser was used to heat the cantilever by computer controlled optical pulses of varying intensity, but of an equal duration of 1 ms. These pulses programmed the different mechanical states. The intensity

of the lasers was measured with an optical power meter (Thorlabs model: PM100D). L1 and L2 are arranged orthogonal to each other so that the light from L2 does not affect the PSD reading, which relates only to the beam reflected from L1. The voltage output from the PSD was amplified by a DC coupled amplifier and filtered for high-frequency interference. All the experiments were done at ambient pressure.

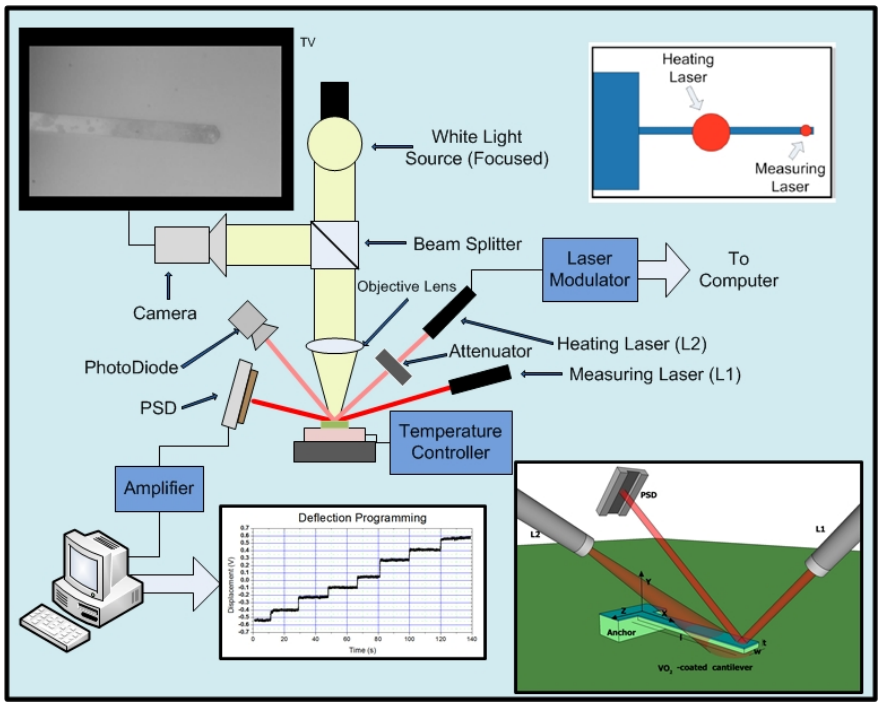

Figure 3.8 Measurement set up. The entire system was in ambient pressure. As shown in the insets, the measuring laser (L1) was focused at the tip of the cantilever, while the heating or programming laser (L2) was focused close to the center of the cantilever beam [8].

Similarly to **Section 3.1 and 3.2** the first step was to characterize the transition, in order to determine the 'operating temperature'. The cantilever deflection was monitored while a PID-controlled Peltier heater (Custom Thermoelectric 03111-9L31-04CG) was used as the heat source - L2 was not used. The temperature was increased in intervals of 0.5 ^oC, and the measurements were taken after the set temperature was reached and stabilized. The result shown in **Figure** 3.9.

The VO_2-coated cantilever was bent downwards at room temperature. As the sample was heated through the SPT, the area of the VO_2 plane parallel to the Si surface was

reduced, causing the cantilever to bend upwards (See **Chapter 2**). The heating/cooling curves showed a rather broad hysteresis for VO_2. However, this was found beneficial for this particular application, since broad hysteresis allow for larger number of memory states. The PSD voltage at 30 and 100 ^oC correspond to the minimum and maximum deflection of the tip of the cantilever, respectively, taking a perfectly flat cantilever as a reference (0 μm). With this information the relationship between PSD voltage output (left y-axis in **Figure** 3.9) and the cantilever tip deflection (right y-axis **Figure** 3.9) was determined.

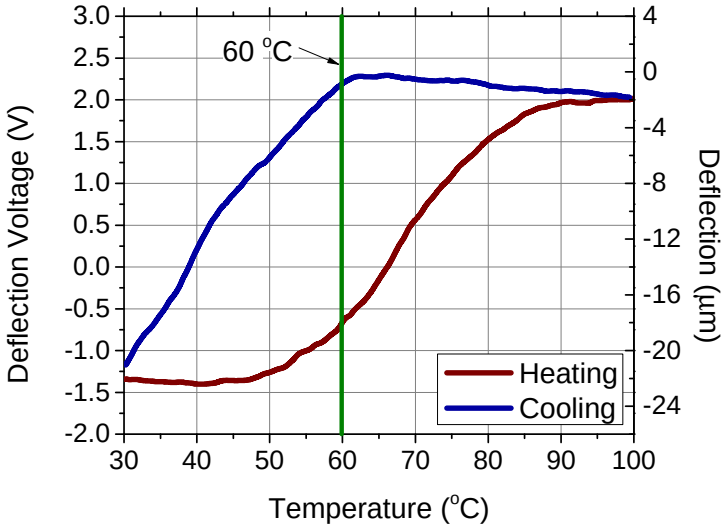

Figure 3.9 Deflection of the cantilever as a function of temperature. A relatively wide hysteresis width for VO_2 thin films of 30 ^oC can be noticed. The left y-axis represents the voltage reading form the PSD, and the right y-axis is the cantilever deflection [8].

In order to obtain more mechanical states, laser pulses with the minimum power that caused a detectable deflection were used in this experiment. Since the minimum intensity from L2 (3 mW) was already beyond this minimum intensity value, optical attenuators had to be placed between L2 and the sample. The minimum power of a 1 ms pulse that caused a detectable deflection on the cantilevers was found to be 1 mW. The cantilever was exposed to a sequence of pulses with powers ranging from 1 to 10 mW (the full range of L2 after the optical attenuators) with increments of 1 mW in order to measure the different mechanical states. The resulting deflection is shown as the blue trace in **Figure** 3.10.

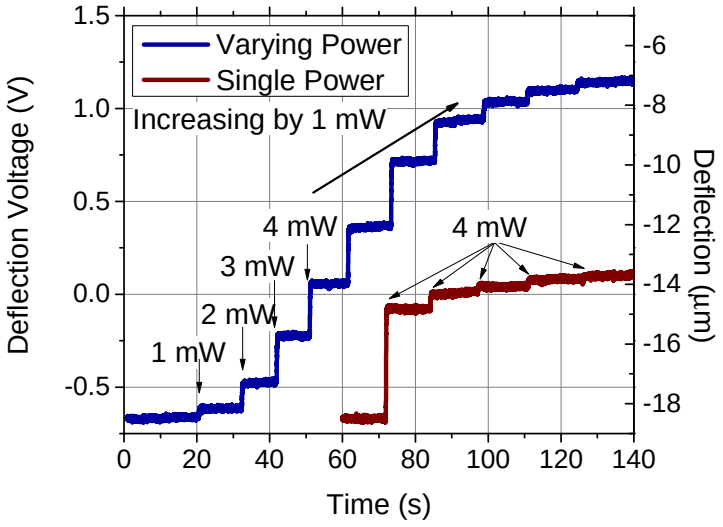

Figure 3.10 Non-uniform mechanical states found from linearly increasing light pulses (blue trace) and for five consecutive light pulses of 4 mW (red trace) [8].

As can be seen, the deflection changed with every pulse, and the new value (i.e. new mechanical state) was sustained until the next pulse started. Of course, this occurred because the "operating temperature" was sustained. It can be noticed in **Figure** 3.10 that the initial deflection (18.5 μm) is very close to the deflection of the major heating curve value at the pre-heating temperature (see **Figure** 3.9). However, the deflection of the final mechanical state (-4 μm) is far from the major cooling curve value at the pre-heating temperature. Furthermore, the change in displacement saturates as -7 μm is approached. As it is explained below, this should not be interpreted as the maximum programmable mechanical memory state being -7 μm.

The bending profile of the two actuation mechanisms (Peltier heating and laser pulse heating) cannot be compared. In the Peltier heating method, the entire sample was in contact with a uniform heat source. The cantilever bending profile in this case had the form of an arc with a radius of curvature that should be similar for VO_2 coated cantilevers with different lengths but otherwise identical. On the other hand, in the laser pulse heating method, the illuminated area of the cantilever was heated much more than the rest. Consequently, the

area of the VO_2 film that transitions from the monoclinic phase to the rutile phase is much smaller for the laser heating method. In this case, the shape of the bent cantilever cannot be best described by an arc. Instead, the bending profile of the laser actuated cantilever had the form of two straight lines joined by an arc. It was also found in a separate experiment that the location of the L2 spot along the cantilever's length defined the cantilever's inflection point. The difference in bending profile between the two heating methods, and the dependence of the total cantilever deflection with the location of the heating laser spot are reasons why the largest deflection obtained with the Peltier heating method (-1 μm) should not be expected when the laser pulse heating method is used. For the programming experiment, the location of L2 (100 μm form the cantilever's anchor), was found empirically to be the location that resulted in the largest deflection.

After these measurements, the cantilever was 'reset' for the next experiment, which consisted on exposure to five pulses of the same amount of power of 4 mW (**Figure** 3.10 red trace). As can be noticed, this resulted in a displacement (or mechanical state) close to the value obtained from the previous experiment after a sequence of 1, 2, 3, and 4 mW laser pulses. This observation suggests that the final value of deflection will be mainly determined by the energy of the pulse. In other words, a specific amount of energy delivered to the cantilever represents a specific mechanical state, which can be stored by traversing a single set or different sets of minor heatingcooling loops.

3.4 Summary

The memory behavior in the optical, electrical, and mechanical properties of VO_2 under photothermal actuation, was studied. Through all three experiments, it becomes evident that in order for the memory behavior to be useful in practical devices, it is necessary to very precisely control the temperature of the samples. Due to the abrupt transition in VO_2, small variations in temperature will cause the 'state' of the material to change. It is also important to notice that the changes in states are very sensitive to the input pulse

energy. Without very precise control of these input pulses it becomes impossible to reliably and repeatably program the 'state' of the VO_2 film. Finally, in all three experiments the material's memory is erased (i.e. reset) by cooling the entire sample to room temperature. In order to program new states, the sample needs to be taken to the "operating temperature" first. Using an external heater for reaching this 'pre-heating' temperature makes the process extremely slow and energy inefficient. The next chapters will discuss methods that will eventually fix (or atleast allevaite) all of these deficiencies by incorporating a micro heater into the MEMS device, and developing a control system that will improve the programing of a VO_2-based memory.

CHAPTER 4

EMBEDDED ELECTRIC MICRO-HEATERS

The previous chapters have presented a detailed discussion of the VO_2 properties, with particular emphasis on the effects of its SPT in MEMS. However, the actuation mechanisms discussed so far include photo-thermal and heat conduction mechanisms that are not very practical for many applications. This chapter presents the development of a VO_2-based MEMS device (a micro-actuator) driven by electric signals through a micro-electric heater (i.e. driven by joule heating). The dynamics of this VO_2-based MEMS device and its design parameters are discussed. Also, a Finite Element Method (FEM) model that integrates the SPT effects into a lumped model is discussed and validated. This model will facilitate the design of future devices by enabling a method to simulate the effects of the SPT. *The work related to this chapter was published in [9].*

4.1 Micro-Cantilever Design and Fabrication

The developed VO_2-based MEMS actuators are composed of SiO_2 with integrated titanium/platinum (Ti/Pt) metal layers, where the Ti layer is only used for adhesion purposes. The first layer of Pt forms the contact pads and traces necessary for either wire bonding or probe electrical connections (wire bonding was used in this work). It also forms a bottom electrode, which could be used for capacitive detection. The second Pt layer forms the integrated heater and provided a reflecting surface, necessary for optical detection (the SiO_2 cantilever is transparent to the wavelength used for optical detection (λ=632 nm)). This second layer of Pt is buried inside the SiO_2 cantilever, electrically isolating the heater from the VO_2 film. This isolation is necessary to avoid a short circuit across the resistive heater when the VO_2 becomes conductive in the metallic phase.

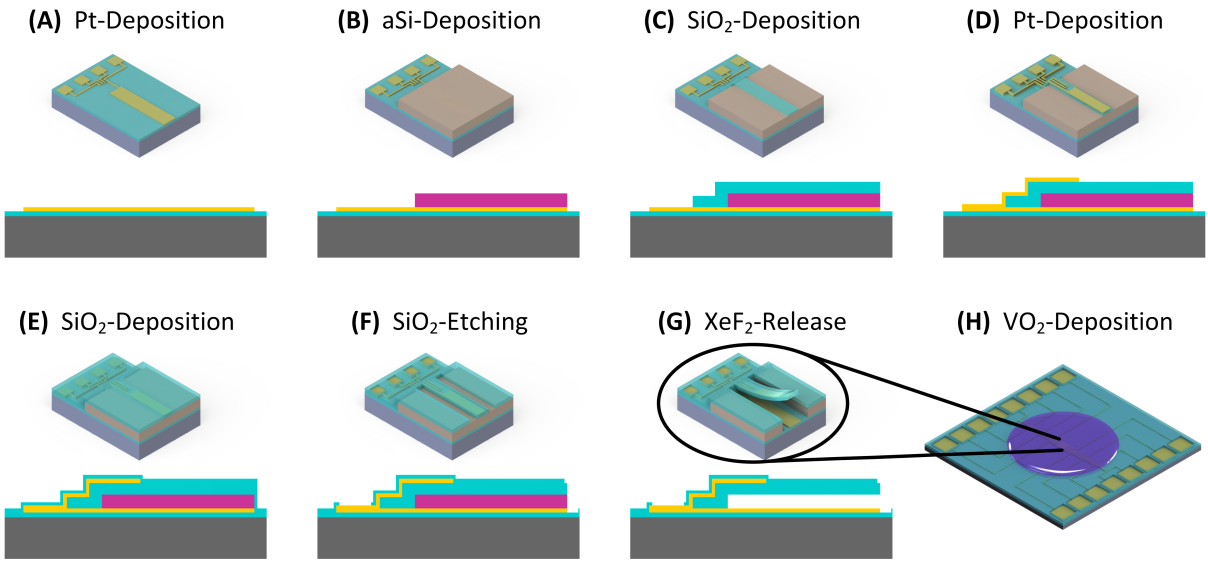

Figure 4.1 General fabrication process flow. (A) Bottom electrode deposition and patterning by lift-off, (B) Sacrificial layer (amorphous silicon) deposition and patterning by RIE, (C) First SiO_2 deposition and patterning, (D) Top electrode deposition (Heater), (E) Second SiO_2 deposition, (F) Patterning of the second SiO_2 layer, (G) Release of the MEMS actuator, and (H) VO_2-deposition by pulsed-lased deposition using in-situ shadow mask [9].

Figure 4.1 shows a general overview of the fabrication process. The starting substrate consisted on a silicon wafer with a 1.2 μm thick layer of silicon dioxide (SiO_2) deposited by PECVD. A Ti (50 nm)/Pt(150 nm) layer was deposited by evaporation and patterned by lift-off. The sacrificial layer (500 nm thick a-Si film) was deposited by LPCVD and patterned by RIE. A second thin layer of SiO_2 (500 nm) was deposited by LPCVD (in order to minimize voids in the cantilever's structural material) and patterned using plasma etching. A second metallization Ti(40 nm)/Pt(150 nm) followed, this time by sputtering (to increase the film's conformity). This second metal layer was also patterned by using lift-off, and it formed the integrated resistive heater. The final layer of SiO_2 (500 nm) was deposited again by LPCVD and patterned using plasma etching. The wafer was then diced and the structures were released using XeF_2, which is a dry (gas, not plasma) etching method.

The final step in the device fabrication is the deposition of the VO_2 thin film (200 nm thick), which was done using a shadow mask to guarantee that VO_2 was only deposited on the area of the chip that contains the suspended cantilever beams and away from the

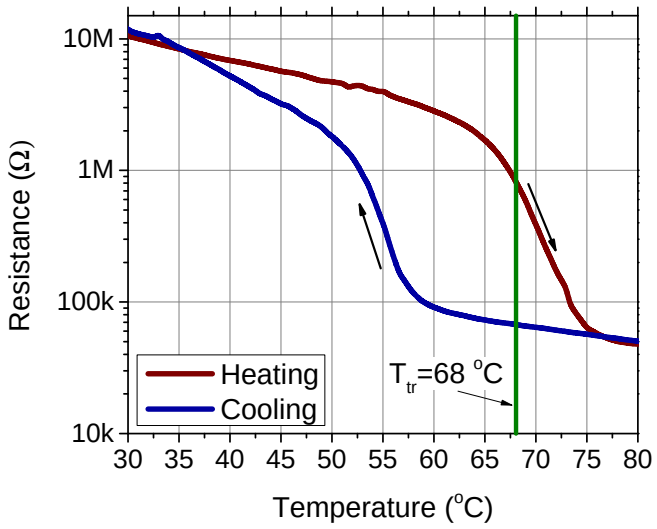

Figure 4.2 Resistance as a function of temperature for the VO_2 film used. The VO_2 film was a circular pattern of 6 mm in diameter, and the probes were 2 mm apart [9].

contact pads. Film quality was verified by measuring the change in resistance of the VO_2 film across the IMT, which showed the typical hysteretic behavior of (see **Figure** 4.2). The finalized device was wire bonded to an IC package for testing. **Figure** 4.3 shows a scanning electron microscope (SEM) image of the two tested cantilevers with their dimensions. The final thickness of the cantilever is approximately 1 μm.

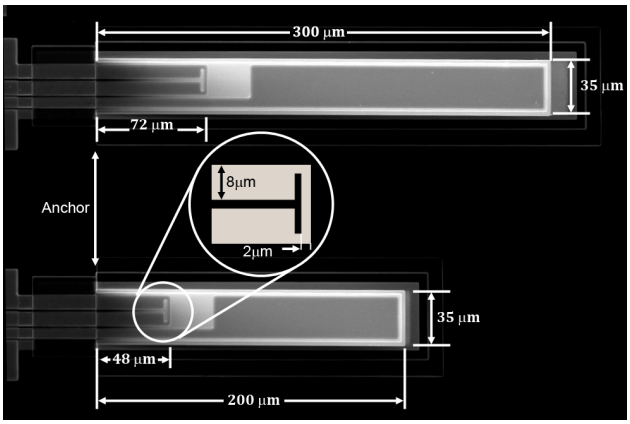

Figure 4.3 SEM image of cantilevers with dimensions (top view) [9].

4.2 Finite Element Model

Although the simulation of the structural changes in a VO_2 crystal could be addressed by modeling of the lattice changes of VO_2 single crystals during the transition, the case for polycrystalline VO_2 is more complicated. Polycrystalline VO_2 consists of multiple layers of VO_2 crystals of different sizes, which do not experience perfectly synchronized structural changes with temperature, and which are not perfectly oriented the induced strain during the phase change is not perfectly uniaxial. Additionally, the modeling of the shift in the transition temperature (T_{Tr}) of VO_2 with stress is no longer possible by using the uniaxial stress obtained from the Clausius–Clapeyron equation as it was demonstrated for single-crystal VO_2 [35].

Therefore, experimental data was used in this work to generate a comprehensive lumped model for VO_2-based MEMS actuators, by fitting a temperature dependent thermal expansion coefficient for VO_2 that emulated the strain induced in the micro-actuator during the phase change. The FEM model was also used to simulate the heat losses during actuation pulses, the design of the resistive heater, and the power dissipated in the heater.

COMSOL Multiphysics was used to create such FEM model. The model includes two coupled physics: solid mechanics with thermal expansion, and heat transfer with joule heating. The dimensions of the simulated structures are those of the tested devices. There are two main heat loss mechanisms in these cantilevers. The first one is the heat loss due to thermal conduction to the substrate through the anchor, and the other through convective heat transfer between the structure and its surrounding. To simulate the anchor losses, the face of the cantilever that is in contact with the anchor was given a constant temperature of 30 ^oC. The natural convection boundary condition was approximated by estimating a heat transfer coefficient. This is determined by empirical handbook correlations [36], which the software calculates automatically. **Table 4.1** shows the properties of Pt and VO_2 used in the model.

The FEM model simulated the contraction of VO_2 during the transition and was used to

Material	VO_2	Pt
Young's Modulus (GPa)	140	169
Poisson's ratio	0.33	0.38
Density (kg/m^3)	4670	21450
Heat Capacity ($J/kg*K$)	700	133
Thermal Conductivity ($W/(m*K)$)	4	71.6
Reference Temperature (^oC)	470	470
Thermal expansion coefficient ($1/K$)	$\alpha(T)$	8.8×10^{-6}
Electrical Conductivity (S/m)	N/A	$\sigma(T)$

Table 4.1 Material properties used in the FEM model.

calculate the electric power dissipated at the Pt heater as a function of temperature. Given that the thermal expansion coefficient of Pt varies less than 2% in the temperature range that includes the phase change in VO_2 [15], this value was assumed to be constant in the analysis. The contraction of the VO_2 thin film, and the power dissipated at the Pt heater as a function of temperature were modeled by a temperature dependent thermal expansion coefficient of VO_2 ($\alpha(T)$) and conductivity of Pt ($\sigma(T)$), respectively. The following expressions were used:

$$\alpha(T) = \frac{6 \times 10^{-6}}{1 + e^{-0.3(T-341.15)}} - 3 \times 10^{-8}(T - 273.15) + 6.9 \times 10^{-6} \tag{4.1}$$

$$\sigma(T) = \frac{8.9 \times 10^{6}}{1 + 0.003729(T - 293.15)} \tag{4.2}$$

where T is temperature in Kelvin. **Equation** (4.1) was obtained from a curve fit to experimental measurements, while the numerator of **Equation** (4.2) is the conductivity for Pt at room temperature, and the expression in itself is commonly used for modeling changes in conductivity as a function of temperature. A plot of **Equation** (4.1) is shown in **Figure** 4.4 . This model was used to estimate the operating current, and the dynamic response of the system under various conditions.

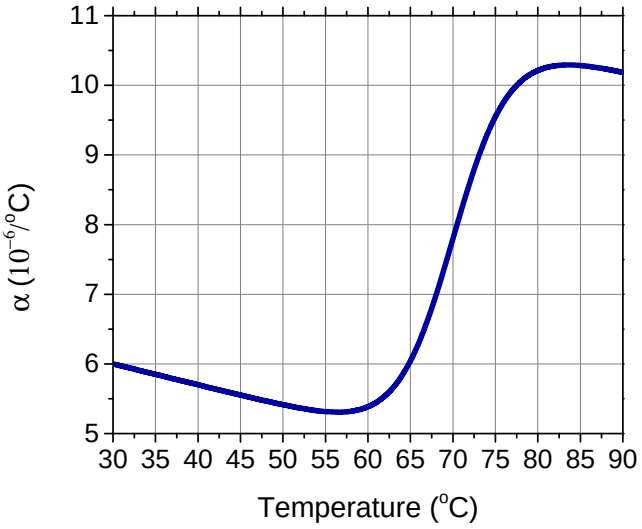

Figure 4.4 Temperature dependent thermal expansion coefficient of VO_2 (plot of $\alpha(T)$ in **Equation** (4.1)) [9].

4.3 Heater Design

The heater was designed to localize the power dissipation as much as possible along the cantilever's length and to maintain a uniform temperature across its width, to avoid twisting when heating. A single thin Pt line was chosen as the heater element, due to its simplicity. The width of this line was 2 μm, which also was the minimum feature size of the fabrication process. The heater was connected to larger electrode pads through wider traces (8.5 μm) in order to concentrate most of the power dissipation at the heating element region (i.e. at the 2 μm wide Pt resistor). Another design parameter was the location of the heater that would maximize the deflection of the cantilever while minimizing power consumption.

As the heater location approaches the anchor, the conductive heat loss through the anchor increases, which increases the power necessary to reach a specific temperature. However, the closer to the anchor the VO_2 film contracts, the greater the deflection of the cantilever. This indicates that the location of the heater involves a tradeoff between power dissipation and cantilever deflection. In this design the location of the heater was optimized. The thickness of the Pt heater also affects the electrical resistance of the heater, and consequently the

power dissipated in the heating element. For the particular device presented here, it was found that a Ti/Pt thickness of 200 nm was large enough to avoid film discontinuities and thin enough to maintain the operating currents within the mA range. The final design was obtained with the help of the FEM simulations discussed earlier.

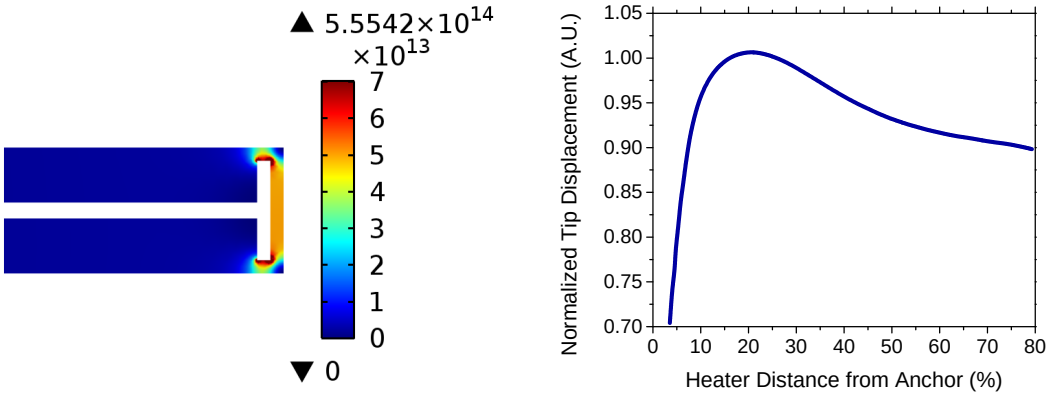

(a) FEM simulation of the power dissipation in the heater, scale is in W/m^3.

(b) Simulation of the deflection of the cantilever as the position of the heater is varied. Optimum position is near 24%.

Figure 4.5 FEM simulation results for heater optimization [9].

Figure 4.5 shows the final heater design as well as the FEM simulations results for power dissipation and optimum location of the heater. The optimal location of the heater was determined to be at around 24% of the cantilever length from the anchor. This result also agrees with previous work, where the optimum position of a heating laser spot was determined, for maximum amplitude [37]. The resistance of the heater was found to vary between 16.5 Ω and 20.5 Ω as the current is increased from 0 to 9 mA.

4.4 Results

The measurements are divided into two main categories: static and frequency response. In the static analysis the relationship between heater current and tip displacement is studied, as well as the difference in power consumption when the system is in vacuum or open to

atmosphere pressure. The frequency analysis studies the bandwidth of the system and the effects of the design parameters.

4.4.1 Static Analysis

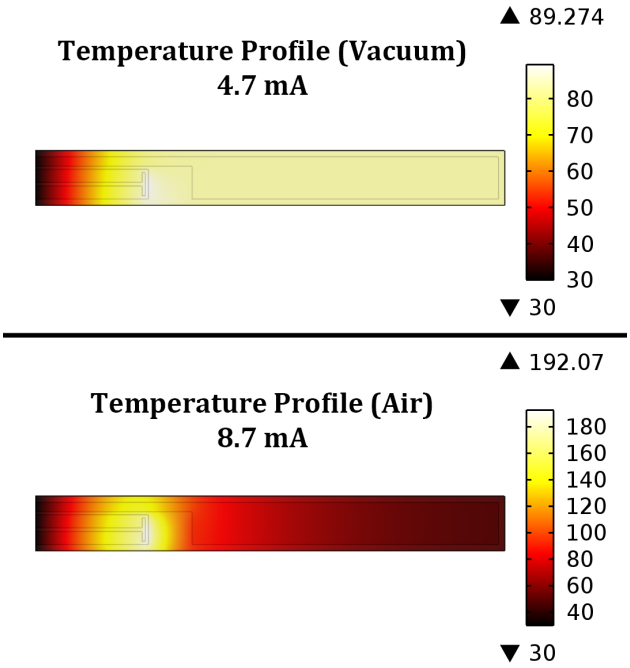

Figure 4.6 FEM simulation results of the temperature (^oC) distribution for the 300 μm cantilever in air and vacuum. The anchor is at the left [9].

Figure 4.6 shows the simulated temperature profiles for the 300 μm long cantilever under vacuum and air. A more uniform temperature over the surface of the cantilever is obtained for vacuum environment. This means that the difference in temperature between the heater and the rest of the cantilever, in vacuum is smaller than in air, and therefore the heater only needs to reach about half the temperature needed in air to obtain the same deflection. Also, the resistance of the heater is smaller at lower temperatures, which translates to less power consumption in vacuum. This was confirmed experimentally as shown below. **Figure** 4.7 shows a SEM picture of both cantilevers before and after actuation under vacuum. There is an initial deflection at room temperature, before actuation, due to the residual stress from

the deposition of VO_2 which occurs at nearly 470 ^oC. The total deflection for the 300 μm and 200 μm cantilevers upon actuation was 68.7 μm and 28.5 μm, respectively.

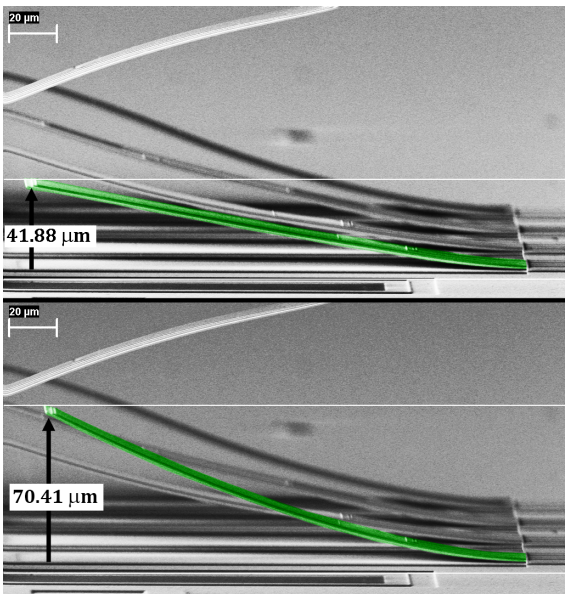

(a) The 200 μm long cantilever (highlighted in green).

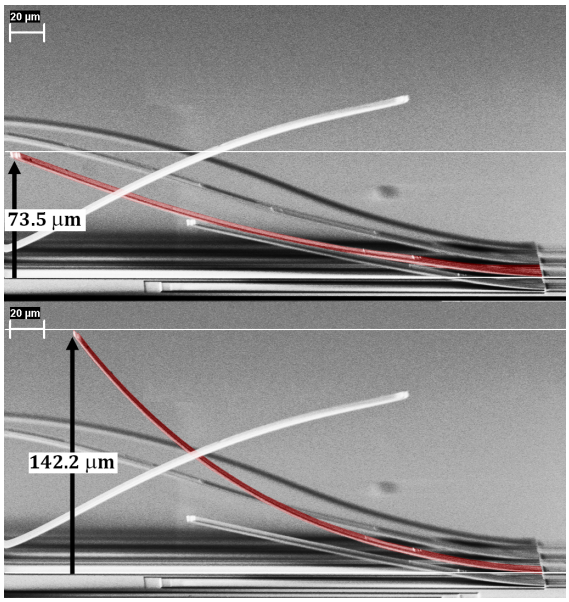

(b) The 300 μm long cantilever (highlighted in red).

Figure 4.7 SEM images of cantilevers. The top and bottom images show the actuator before and after actuation, respectively [9].

Figure 4.8 shows the deflection as a function of input current for both cantilevers. The deflection measurements were taken from SEM images as the current to the resistive heater was increased in increments of 0.4 mA. The electrical signals for this experiment were provided by a voltage-to-current converter connected to the chip inside the SEM by electrical feedthroughs.

It can be seen that the simulation correctly predicts the deflection and general shape of the response, but it is shifted towards larger current values, which represents an overestimate of the actual heat loss in the system. The experiment in air is closer to the simulation results, which shows that the overestimate is more likely due to the modeling of the anchor losses than to the modeling of the heat convection. The FEM model assumes perfect anchor geometry, which does not exactly represent the real system, since the metal and SiO_2 depositions are not perfectly conformal. This non-conformity results in a cantilever structure with a smaller

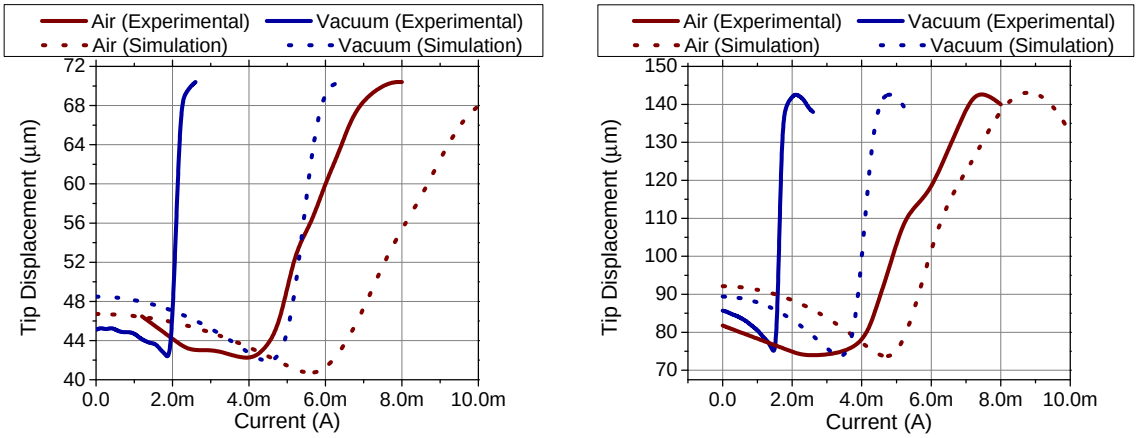

(a) 200 μm long cantilever.

(b) 300 μm long cantilever.

Figure 4.8 Static response and FEM simulation results in vacuum and in air [9].

cross-section at the anchor, making the actual cantilever more thermally insulated from the substrate than the FEM model. It can also be noticed that, in air, the difference in operating current between the simulation and the real system is less than 10% of the full range for the 300 μm-long cantilever; while this difference is about 20% for the 200 μm-long cantilever (see **Figure** 4.8). This indicates that the error in FEM model predictions becomes larger as the heat losses through the anchor become more dominant (the 200 μm-long cantilever has a lower surface-to-anchor area ratio). It is also noted that the displacement curves across the phase-change are steeper for the device operated in vacuum media. This is because a given increase in current will produce a larger increase in temperature for the device in vacuum, since convection losses are almost non-existent.

Another observation can be made in terms of power consumption. Taking the average of the simulated change in resistance for the Pt resistive heater mentioned earlier (18.5 Ω), and the experimental measurements shown in **Figure** 4.8, an estimate of the required power to achieve full-actuation can obtained. These results are summarized in **Table 4.2**. It is noted that the necessary current to achieve full-actuation in air was approximately 3 times larger than in vacuum, which means that full actuation in air requires approximately 16 times more power than in vacuum.

Environment	Estimated Required Power for Full Actuation (mW)	
	300 μm Cantilever	200 μm Cantilever
Vacuum	0.07	0.09
Air	1.15	1.18

Table 4.2 Estimated Power Consumption

4.4.2 Frequency Response

The schematic of the set-up used for the frequency response measurements is shown in **Figure** 4.9. The set-up is based on laser deflection (or light scattering) techniques, similar to those used in the past [38]. A network analyzer (Agilent 3589A), was connected to an adjustable voltage to current converter. A HeNe laser (CW 632 nm) was focused on the cantilever inside a vacuum chamber. The reflected beam was detected using a silicon photodiode (thorlabs PDA10A) and a DC-300 MHz amplifier (Stanford Research Systesm model SR445). The vibration of the cantilever generates oscillatory movements of the reflected laser beam, which the photodiode converts to an oscillatory voltage signal detected by the network analyzer for determining the frequency. A CCD camera was used for facilitating laser alignment prior to the measurements. The cantilevers were operated using a positive sinusoidal current with adjusted amplitude and offset values to guarantee that the cantilevers remained inside the SPT. This was monitored through an oscilloscope (Tektronix TDS2004C) connected directly to the photodiode.

During the frequency response measurements, it was found that the He-Ne laser used for detection heated the cantilever structure due to optical absorption. Since the cantilevers are thermally isolated from the substrate, this power absorption added additional heat flow into the cantilever besides the heat created by the resistive heater. Therefore, care was taken to ensure that the laser spot was always placed close to the resistive heater, and a neutral density filter was placed between the He-Ne laser and the first beam splitter, so that the minimum amount of intensity necessary that allowed vibration detection from the reflected

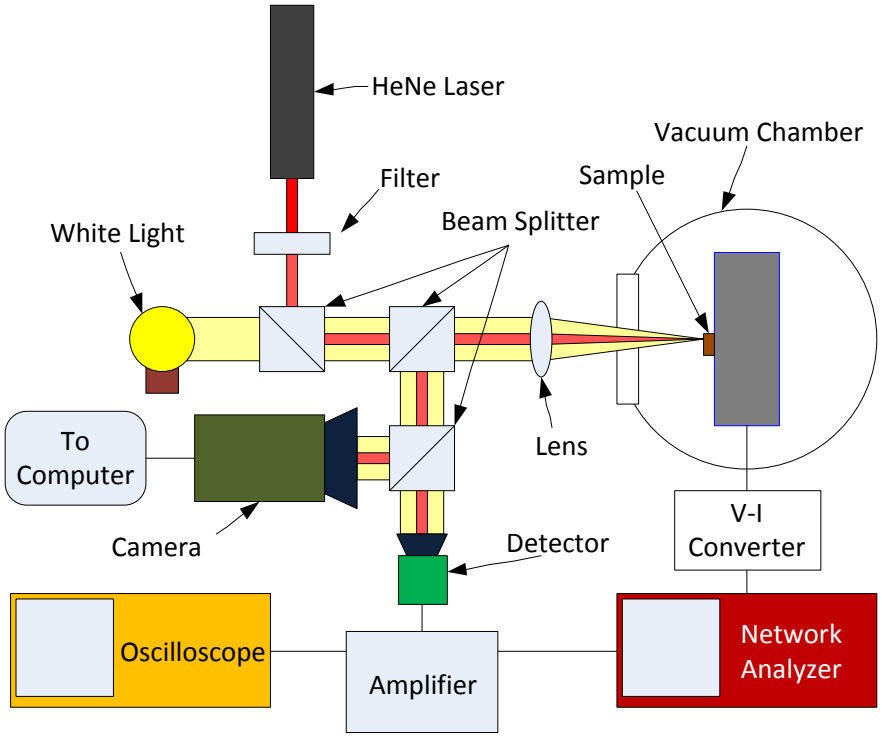

Figure 4.9 Schematic of system used for frequency measurements [9].

laser beam was used. It is reasonable to assume that the delay between the mechanical response and the thermal response is negligible since the air damping effects don't become significant until the cantilever is actuated at higher frequencies and the SPT of VO_2 is much faster [39]. Therefore, the most important effect to consider in electro-thermally driven VO_2 actuators is the dynamic response of the heat transfer in the cantilever. The model that was used to analyze the frequency response of the cantilevers includes heat transfer and joule heating mechanisms.

Figure 4.10 shows the frequency response of the cantilevers. These results show the cut-off frequency as defined by a 3 dB drop in amplitude (half power) with respect to the maximum amplitude at low frequencies. The frequency range was chosen to include the first resonant mode of the cantilever, which is shown as a peak in the response close to 10 kHz. A lower quality factor is observed for the measurements done in air, which suggests that air damping dominates the energy losses, as expected.

The cut-off frequency increases when the cantilever is exposed to air, which suggests that

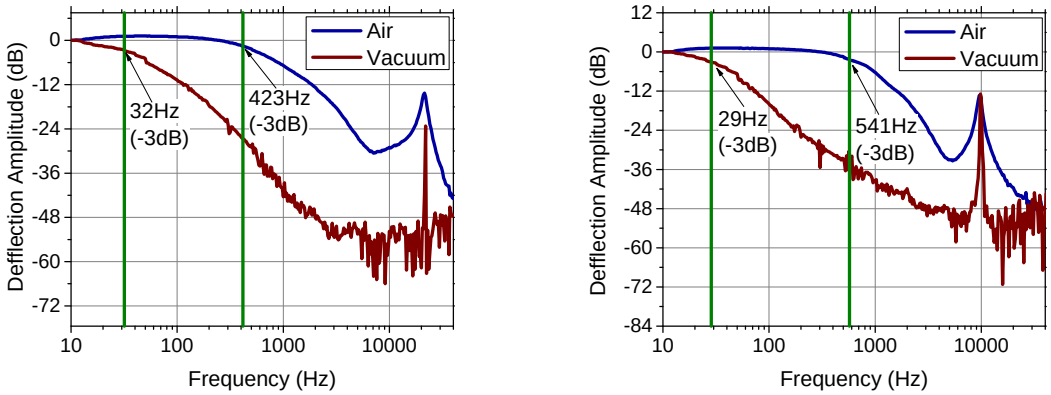

(a) The 200 μm long cantilever.

(b) The 300 μm long cantilever.

Figure 4.10 Frequency response curves for the cantilevers in vacuum and in air [9].

the limiting factor when it comes to half-power frequency response is dominated by heat convection losses. For the two cantilevers in vacuum, the difference in heat dissipation by conduction through the cantilever's anchor is minimal, since the anchor area is the same for both cantilevers. This is shown by very similar cut-off frequencies in vacuum where the difference is only 9%. In air, however, there is a larger difference in cutoff frequency (about 25%), which is also supportive of the suggestion that heat convection losses dominate the cut-off frequency, since both cantilevers have different surface areas. This indicates that when operating in vacuum or very thermally isolated conditions, the size of the cantilever affects very little the cut-off frequency of the cantilevers as long as you are operating the cantilever far below the resonant frequency.

4.5 Summary

This chapter discussed the development of a VO_2-based actuator with an embedded micro electric heater used for actuation. The performance of this actuator (static and dynamic behavior) was characterized. FEM Models where developed and validated that will facilitate future VO_2-based MEMS transducer designs. The necessary current for maximum deflection was found to be very dependent on the ambient conditions particularly external pressure

and temperature. In order to be able to precisely control the displacement of these types of actuators, feedback control must be used to compensate for external ambient conditions. This control issue is the subject of the next chapter.

CHAPTER 5

CONTROL OF THE MEMORY EFFECT

In **Chapter 4** it was shown that of the behavior of VO_2-based transducers is very sensitive to variations in external ambient conditions. This is especially true when operating VO_2-based transducers near the hysteretic region, where even a small temporary disturbance will change the state of the VO_2 film. This chapter presents a closed loop system which can be used to compensate for variations in external ambient conditions without further complicating the MEMS device fabrication or design. This technique will be combined with the results from **Chapter 3** to create a VO_2-based MEMS memory cell with much better performance and controllability than previously reported devices. *The work related to this chapter was published in [10].*

5.1 Design of the memory device

The memory cell described in this chapter consists of a VO_2/SiO_2 bimorph cantilever with an embedded titanium-platinum heater, where the titanium is only used for adhesion purposes. The thickness of the heater and its "on-chip" electrical connections (hereby referred to as "traces") to the metal contact pads is 200 nm. A top view of the device can be seen in **Figure** 5.1. The thickness of the cantilever was $2\mu m$ and the thickness of the VO_2 film was approximately 200 nm. The chip was cemented to an IC package using silver paint and gold wires were bonded from the Ti/Pt metal pads on the chip to the connections of the IC package, through which all the actuation and feedback electrical signals are transmitted.

Because of the large linear sensitivity of the resistivity of Pt to variations in temperature, it is possible to use the resistance of the heater as a feedback measurement to stabilize the temperature of the cantilever. **Figure** 5.2 shows how the resistance of the device varies as the temperature is raised from 30 to 85 ^oC. This change in resistance with temperature was

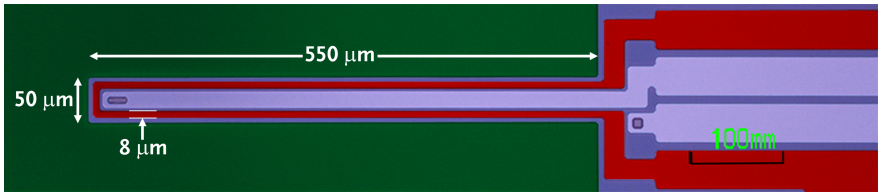

Figure 5.1 Top view false color image of the memory cell. The Pt/Ti heater is shown in red [10].

used on later experiments to monitor the temperature of the microcantilever. The entire device can be actuated and controlled through this single terminal, simplifying the complete system.

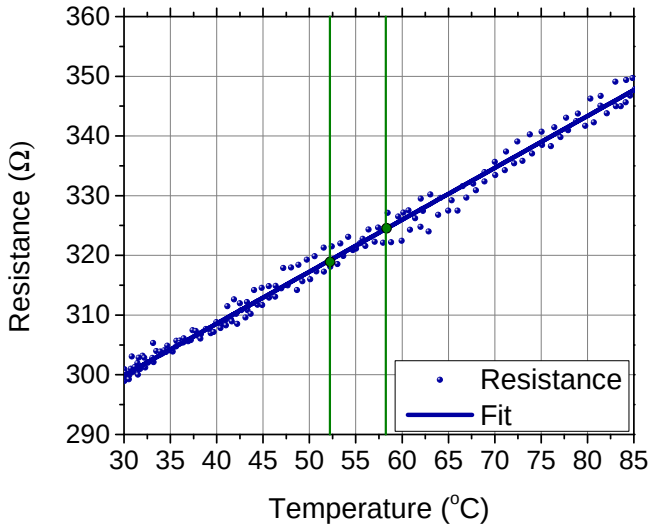

Figure 5.2 Measured resistance of the heater (and connecting traces) as the temperature of the entire chip is varied [10].

After deposition of the VO_2 film, the deflection of the cantilever was characterized as the substrate temperature was varied across the SPT window. The results are shown in **Figure** 5.3. The transition temperature in this work is defined as the points in the heating and cooling curves where the rate of change in deflection is the largest. The transition temperature for the heating and cooling curves are marked in green, and the corresponding device resistance is also marked in **Figure** 5.2. This curve shows the classical curve for the SPT found in previous work, showing that we have a highly oriented film of VO_2. Since the

temperature sensor used to measure the temperature of the IC package was placed on the IC package instead of directly on the die, conductive losses from the device to the sensor resulted in a lower temperature reading. On a separate experiment, the resistance of the VO_2 film was measured as its temperature was varied across the phase transition, and the curve was found to be shifted approximately 10 ^oC higher, which matches the typical transition temperature for VO_2. Because of residual stress during fabrication, there is an initial out-of-plane deflection of the cantilever at room temperature. All deflection measurements obtained were relative to that initial deflection. The static and transient response analysis discussed next is done using electro-thermal actuation (i.e., Joule heating).

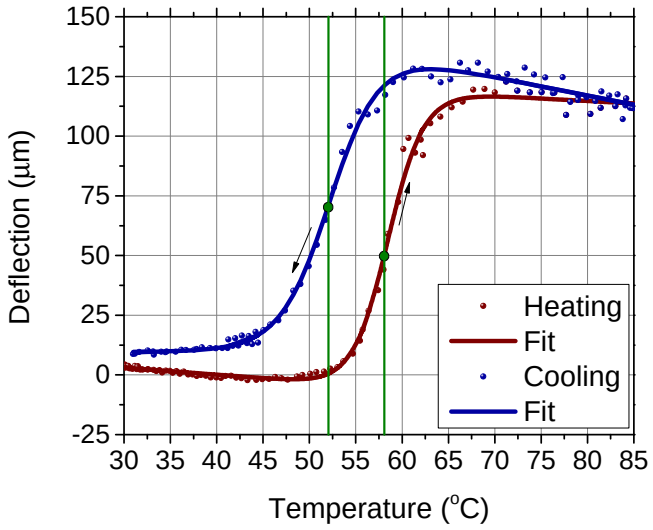

Figure 5.3 Measured deflection of the device as the temperature of the entire chip is varied [10].

5.2 Static and transient response

The deflection of the cantilever was measured as the current through the device was cycled from 0 to 7 mA. **Figure** 5.4 shows the resulting deflection curve. It can be readily noticed that the shape of the deflection curve in **Figure** 5.3 and 5.4 are different. This is due a change in temperature distribution when heating with the integrated heater in the cantilever, vs.

heating the whole chip with the Peltier heater. In conductive actuation, the Peltier heater covers the entire bottom surface of the chip and therefore, the temperature is very uniform across the entire chip. However, in the case of Joule heating, only the suspended structure is being heated and the cantilever's anchor acts as a heat sink.

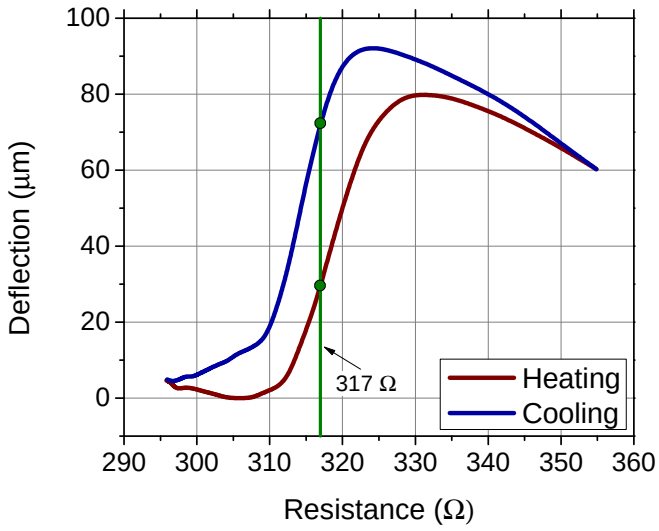

Figure 5.4 Deflection of the cantilever as the current is cycled, the deflection is plotted as a function of the device resistance [10].

The total measured resistance of the heating electrode can be considered as two electrical resistances connected in series: (i) the resistance of the heating element, and (ii) the resistance of the traces. It is necessary to estimate the values of these two resistance components, since they can not be physically measured directly (note the size of the cantilever and the dimensions of the heater and traces in **Figure** 5.1). The data from previous curves and the dimensions of the heater were used for this calculation, and heater resistance was found to be 216 Ω whereas the trace resistance was found to be 84 Ω (both values at room temperature). The thermal coefficient of resistance (TCR) of the Ti/Pt metallization was measured to be $3.17\times10^{-3}\ K^{-1}$.

As discussed in **Chapter 3**, the presented VO_2-based MEMS memory device is required to operate within the hysteretic region. In order to maximize programmable states, it is best

if the device is preheated to a value at which the distance between the outermost hysteretic loops (heating and cooling) is largest [8, 40]. In **Figure** 5.4 the outermost loops are the red and blue lines, and the optimum operating resistance is shown by the green line, 317 Ω in this case. The vertical separation of the loops at this resistance is the theoretical maximum difference between the memory "states", 44 μm in this case. The current needed to maintain this operating temperature when the device is at 30 ^{o}C is 3.6 mA and the resistance of the heater is 233 Ω which gives us the average power needed to operate the device at room temperature, 3.02 mW.

In order to maintain the operating resistance of the device under fluctuating ambient conditions, a closed-loop controller for the system was designed and implemented. For the design of the controller, it was necessary to know the time response of the system. All the control design parameters (e.g., sampling time, duration of programming pulses, etc.) will depend on the speed of the system, which is limited by how fast can the temperature of the structure be changed (see **Section 4.4.2**). A full scale open-loop current step response is shown in **Figure** 5.5.

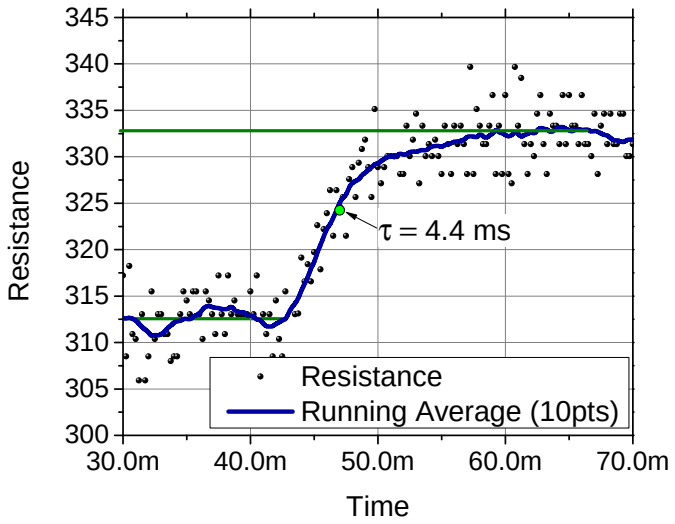

Figure 5.5 Step response of the measured resistance of the device. Scattered points are individual data measurements, and solid curve represents the average of the previous 10 resistance measurements [10].

The measured time constant was calculated from the average curve to be 4.4 ms. In order to guarantee that the structure achieves a steady-state temperature after a step input, the duration of the programming pulses were 40 ms which is several times larger than the times constant. To have a more robust system that can compensate for temperature fluctuations, a feedback system was designed, where the device's temperature is constantly monitored and used to control the current supplied to the heater. The closed-loop system should be independent on the programming pulses; and thus, it was designed to be 10 times slower than the programming pulse (400 ms). The control system was implemented using a field programmable gate array (FPGA).

5.3 Open-loop versus closed-loop behavior

Figure 5.6 shows the schematic of the circuit used and the block diagram of the control system. The programming pulses are added to the output of the controller (which is limited to voltage amplitudes between 1 and 10 V). The device (represented by R_D in the schematic) was connected in series with a known resistance (R_1) of 1.2 $k\Omega$. The value of R_1 was chosen to protect the resistive heater in the actuator by limiting the current due to the maximum applied voltage of 10 V. Using the measured value for the voltage across R_1 and simple circuit analysis, the current through the device and the value for R_D was calculated ADD $R=V/I$. The controller setpoint R_{Set} is set to the previously determined operating resistance 317 Ω.

The first memory experiment was designed to test the robustness of the system. The temperature of the chip was maintained at 30 ^oC using the Peltier, while the closed-loop control system maintained the device resistance at 317 Ω. Then, programming current pulses that maximized the difference in states were applied. In order to maximize the difference in the programmed mechanical states, the pulse had to be large enough to transition the phase change region completely during heating and cooling. The amplitude of the pulses required were +1.52V (for heating) and -3V (for cooling). A train of pulses that cycled between the

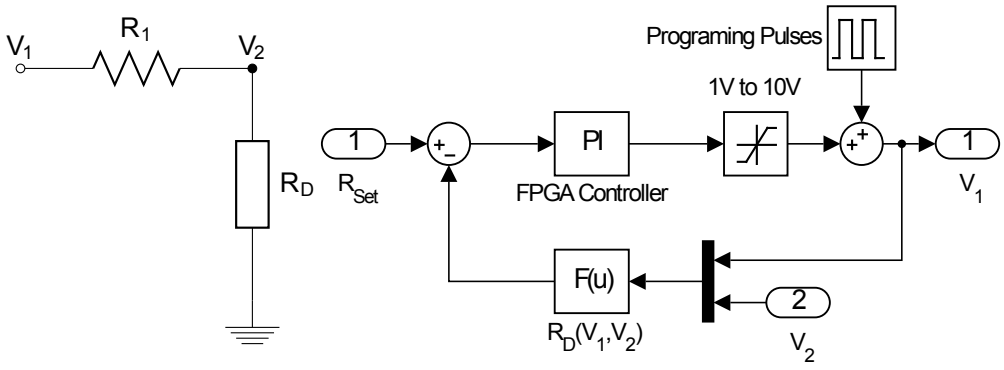

Figure 5.6 Circuit schematic showing how the device is connected, where the voltages are read, and a block diagram of the FPGA controller [10].

two states was applied, and the result is shown in **Figure** 5.7. This experiment was repeated when the chip is at a temperature of 40 ^oC (result also shown in **Figure** 5.7).

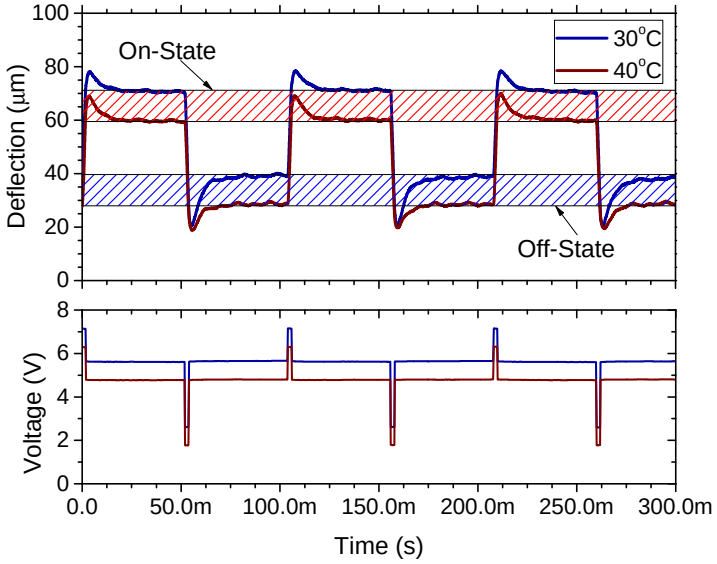

Figure 5.7 Close-loop response of the device at 30 and 40 ^oC [10].

In memory devices it is important to be able to differentiate between the different states, for example, by using a comparator with a threshold somewhere between the states. This means that at all times the states of a memory device must remain inside certain "windows" that must never overlap. **Figure** 5.7 shows that as the temperature is raised the states shift down by a small amount, but they remain inside windows that are separated by a sufficiently large amount that permits reading of the states independently from temperature.

An important detail to notice is that for the higher background temperature of 40 ^oC, the steady-state deflection is lower. However, from **Figure** 5.3 and 5.4, the steady-state deflection should be larger for a higher temperature. This can be explained by considering that the resistance of the device, R_D, is actually composed of two parts as explained before,

$$R_D(T, V) = R_{trace}(T) + R_{heater}(T, V) \tag{5.1}$$

Where R_D is the measured resistance of the device, T is the ambient temperature in ^oC, V is the magnitude of the applied voltage pulse, R_{heater} is the resistance of the heater in the device, and R_{trace} is the resistance of the Ti/Pt traces, given by:

$$R_{trace}(T) = 84\Omega[1 + TCR(T - 30^oC)] \tag{5.2}$$

Notice that R_{trace} has been assumed to be only a function of the ambient (or background) temperature (i.e., the traces are assumed to be perfect heat sinks). From these two equations, it can be noticed that when the ambient temperature rises by +10 ^oC, R_{trace} increases by 2.6 Ω and since the controller forces R_D to remain at 317 Ω, the value of R_{heater} has to decrease by the same amount of 2.6 Ω. From the data plotted in **Figure** 5.4 it can be calculated that, a drop of 2.6 Ω from the operating resistance of 317 Ω corresponds to a drop in deflection of approximately 14 μm; which matches the difference in deflection between the steady-state deflection values for the two different background temperatures shown in **Figure** 5.7. Therefore, the difference between memory states at different background temperatures can be reduced by reducing the ratio of R_{trace}/R_{heater}.

It is important to demonstrate the advantages of the designed closed-loop system over the simpler open-loop version. To this end, the same tests were performed on the device in open loop, with a constant average operating voltage that only keep the device resistance at 317 Ω in room temperature. This voltage was 5.65 V. The device was exposed to the same sequence of pulses. The results are shown in **Figure** 5.8.

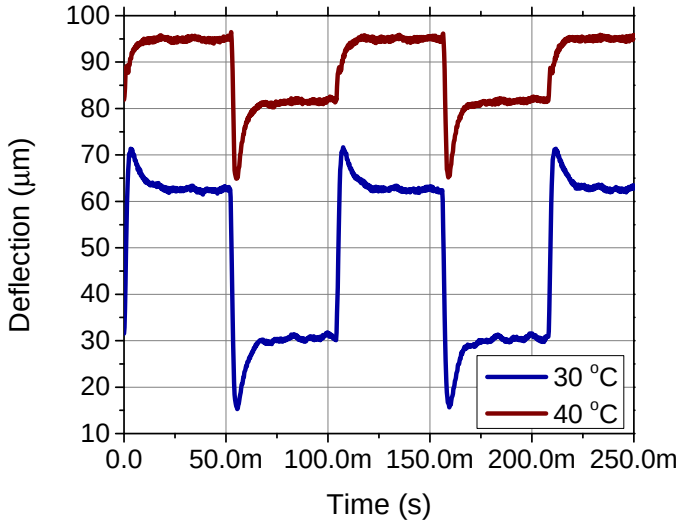

Figure 5.8 Open-loop response of the device at 30 and 40 ^{o}C [10].

At 30 ^{o}C the resulting memory states were very similar to the closed loop response, but when the temperature was raised by +10 ^{o}C the deflection curve shifted up by more than 40 μm. The separation between states for the 40 ^{o}C background temperature is half of that for the 30 ^{o}C. Furthermore, with these new curves it is impossible to set a threshold to differentiate between the two states of the device. Therefore, due to the abruptness of the changes in the properties of VO_2 with temperature, some method for temperature compensation (like the closed-loop system used here) is necessary for practical VO_2-based memory applications.

5.4 Performance of the Vanadium Dioxide-based MEMS memory

The next set of experiments were designed to characterize the reliability of the device, and its multiple state capability. The device was continuously cycled between its two states for 10 min (approximately 12 000 cycles). The values of the two states before and after the cycling were measured and are presented in **Figure** 5.9. After cycling, no noticeable change in the deflection for each state, nor in the shape of the devices response to the programming pulses were noticed.

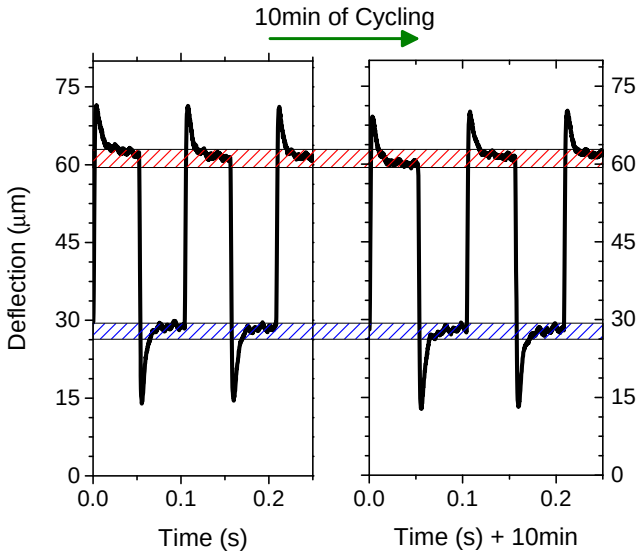

Figure 5.9 Repeatability test of the memory device in close loop [10].

Finally, multiple memory states were demonstrated by controlling the amplitude of the programing pulse. A sequence of positive and negative pulses were used, and the results are shown in **Figure** 5.10.

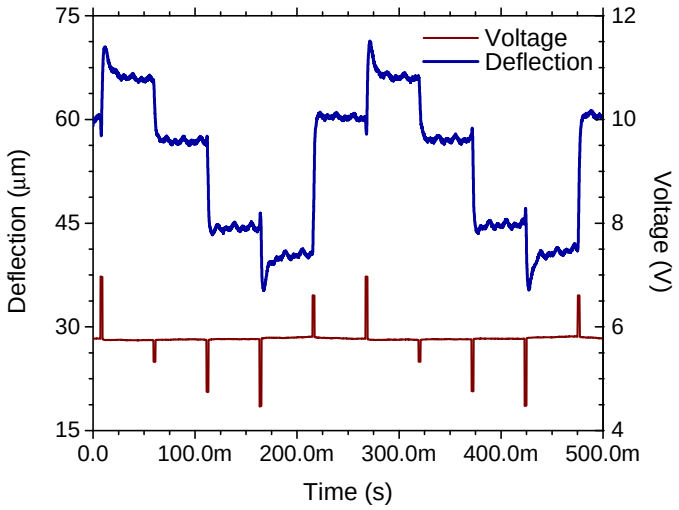

Figure 5.10 Demonstration of multiple stable states in closed loop [10].

5.5 Summary

This chapter presented a VO_2-based micro-electro-mechanical memory cell with a closed-loop system, which used the resistance of the integrated heater as a feedback variable, used to compensate for variations in external ambient conditions, without further complicating the MEMS device design or fabrication. This feedback system also expanded the usable temperature window of the device. The various system parameters that affect the design and tuning of the control loop were studied by determining the static and transient response of the device, and the necessity to operate the device in close loop was demonstrated. A large difference between the programed deection states was shown (30 μm) as well as the capability to demonstrate multiple programmable states. The final memory cell showed high reliability by showing no degradation after 12 000 cycles.

CHAPTER 6

MEMS COMPATIBLE FABRICATION PROCESS FOR VANADIUM DIOXIDE

All the experiments in previous chapters consisted of a continuous VO_2 thin film deposited over the entire device or substrate as a last step in the fabrication process. This is due to the incompatibility of VO_2 with most CMOS of even MEMS fabrication processes. Although many different and useful devices can be fabricated this way, it limits the development of more complicated systems that could benefit from the inclusion of VO_2 films. The high temperature deposition of VO_2 as well as its ability to oxidize or reduce to other stable oxides of vanadium makes it difficult to include it in standard fabrication processes. However, by carefully choosing the right materials and defining a specific process flow, it is possible to deposit and pattern VO_2 films, as well as including them in more complicated MEMS fabrication processes. This chapter presents a case study where a more elaborated process flow is used which includes VO_2 film deposition and patterning as part of an intermediary step. The discussion presents the difficulties of using VO_2 in MEMS processes as well a possible ways to overcome them.

6.1 Vanadium Dioxide-based Voltage Controlled Resistor

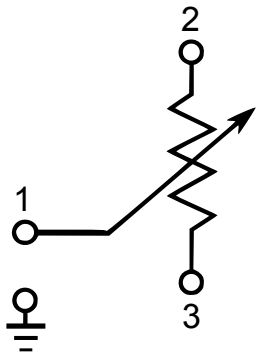

Figure 6.1 Schematic symbol of a VCR.

The device presented in this case study is known as a Voltage Controlled Resistor (VCR).

A VCR is an electronic device which allows the control of a resistance between two terminals by the control of a voltage on a third terminal. Its schematic symbol can be seen in **Figure** 6.1. Ideally the controlled resistance would be independent of the current going through it, and should work for positive and negative voltages, limited only by power dissipation and dielectric breakdown. The controlled resistance should also have a linear relationship with the control voltage. This behavior is summarized in **Figure** 6.2.

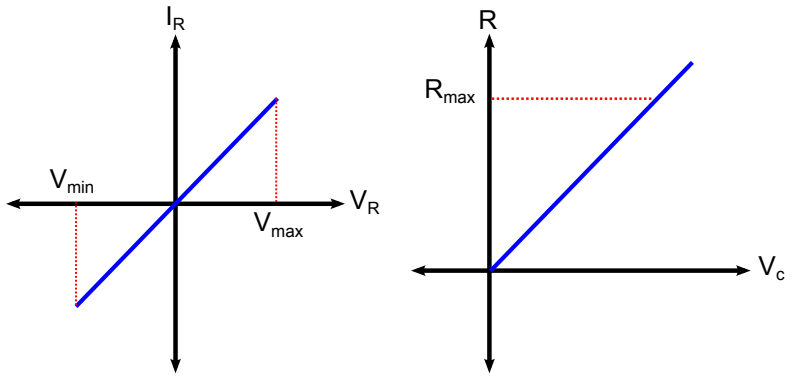

(a) I vs V curve for controlled resistance.

(b) Resistance vs. control voltage.

Figure 6.2 Characteristics of ideal VCR

It is important to note that this device does not exist and, as it will be shown, even the presented device still falls short of this description. However, there are many benefits to implementing this device using VO_2. This device has many applications which include; Variable Gain Amplifiers, Voltage Controlled Oscillators, Automatic Gain Controllers, Low Distortion Tunable Filters, Audio Dynamic Range Compression, and Electronically Controlled Phase Advance and Retard Circuits.

6.2 Device Design

Figure 6.3 shows a general schematic view of the device. The fabricated device consists of the elements presented in (blue), (red), and (green).The circuit connected to the device (shown in black) is used to linearize the response of the VCR. The device consists of two identical VO_2 resistors that are electrically isolated from each other but in thermal contact. One

of them is used to monitor temperature (hereinafter referred to as the "feedback resistor"), while the other is the actual VCR. The two resistors are also in thermal contact with a resistive heater. By controlling the power delivered to the heater, the temperature of the VO_2 can be varied and therefore the resistance can be controlled. Because of the thermal contact between both resistors, we can assume they both have the same resistance. It is also important to consider that when a current flows through the resistor being used in the application the temperature of that resistor will rise due to Joule heating. However, since both resistors are in thermal contact, the temperature of the feedback resistor will also rise, and be detected and corrected by the feedback circuit.

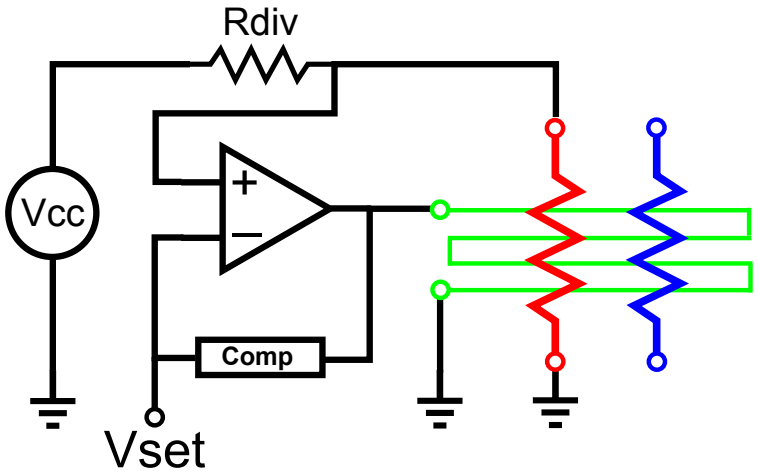

Figure 6.3 Schematic of the VCR device connected in feedback for linearization. blue (VCR), red ("feedback resistor"), and green (resistive heater).

An initial design that was tested involved using two VO_2 films deposited one over the other, separated by a SiO_2 layer. Due to the sensitivity of the oxidation level of the VO_2 films to the annealing time and deposition temperature, the quality of the first VO_2 film was degraded during the deposition of the second film; most probably due to over-oxidation. In order for the VCR to function properly, both VO_2 resistors would need to be identical. So even if this degradation could be reduced, it would be very difficult to achieve two identical VO_2 films that were not deposited simultaneously. Therefore the final process flow must only include one deposition of VO_2.

There are two main components to the VCR: the electric micro-heater, and the VO_2 resistors. The design of the VO_2 resistors requires the characterization of the conductivity of the VO_2 films. This was accomplished by depositing a rectangular patch of VO_2 over SiO_2 using a shadow mask. Aluminum electrodes where then deposited on the sides of the rectangular patch, and the resistance was measured as a function of temperature. The dimensions of the patch as well as the thickness of the VO_2 film was used to calculate the resistivity of the film. The result is shown in **Figure** 6.4.

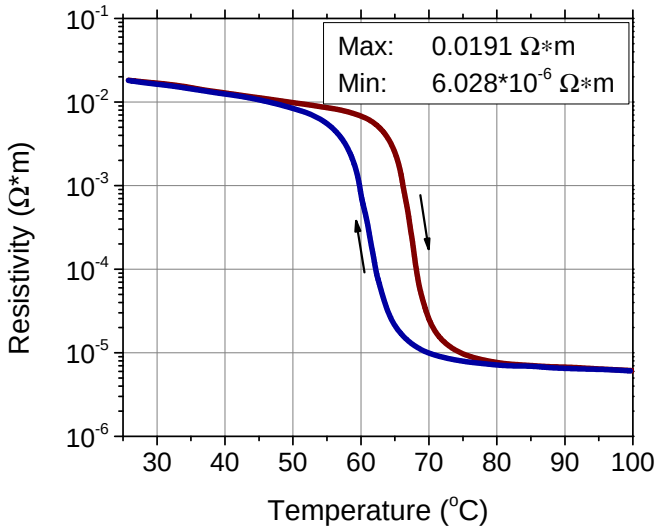

Figure 6.4 Resistivity of a 187 nm thick VO_2 film.

With this curve, a VO_2 resistor can be designed by choosing the appropriate (L/W) ratio. The amount of power needed to raise the temperature of the resistor would depend on its heat dissipation, which is dominated by the surface area $(L \times W)$. However the relationship between the surface area of the resistor and the power needed to raise the temperature by a given amount is difficult to determine analytically, especially for a resistor made of VO_2. So Finite Element Models (FEM) where used to simulate the thermal response of the device. This was combined with experimental measurements shown in **Figure** 6.4 to determine empirical design equations that could be used to calculate the dimensions of the resistors. The dimensions of the resistors were calculated so that for a chosen amount of power they

would reach 100 ^oC.

Any material used in the fabrication process before the deposition of the VO_2 film needs to be able to withstand the high temperatures attained during the deposition of VO_2. For this reason, platinum was chosen for the heater. The design of the heater was much simpler than the design of the resistors. A serpentine pattern was chosen, which covered the entire area of the resistor. The total resistance of the heater was chosen based on the chosen power and chosen operating voltage, and the total number of turns was chosen to match that resistance. The performance of the heaters were also verified through FEM simulations. All FEM simulations were done using COMSOL Multiphysics.

Because only one layer of VO_2 can be deposited on the device, the resistors had to be on the same plane. In order to maximize the temperature uniformity over both resistors, the design shown in **Figure** 6.5 was used. The VO_2 resistors, shown in purple, are broken apart into thin strips which are alternated and connected in parallel. the metal interconnects, shown in yellow would be separated by a thin oxide layer, shown in light blue. The parallel combination of these strips would produce the desired resistance.

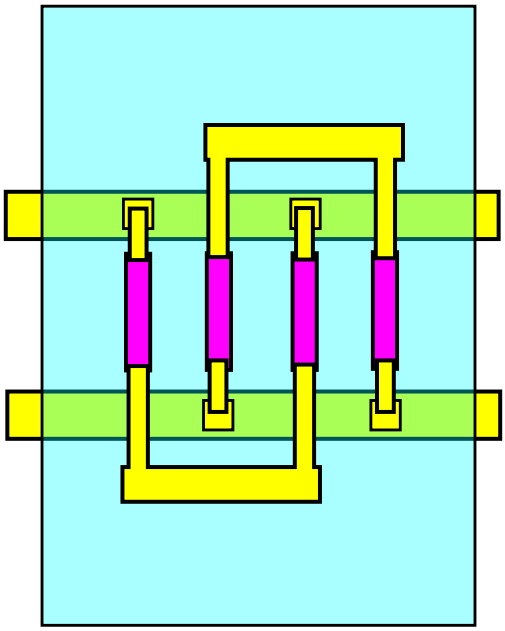

Figure 6.5 Top view of the interdigitated resistive array design used.

6.3 Mask Design

Various designs were implemented. Three maximum resistance values where chosen (200K, 500K, 1M) as well as three maximum power ratings (50mW, 100mW, 200mW). Mask files where designed in L-Edit. **Figure** 6.6 shows an example of one of the devices that where designed.

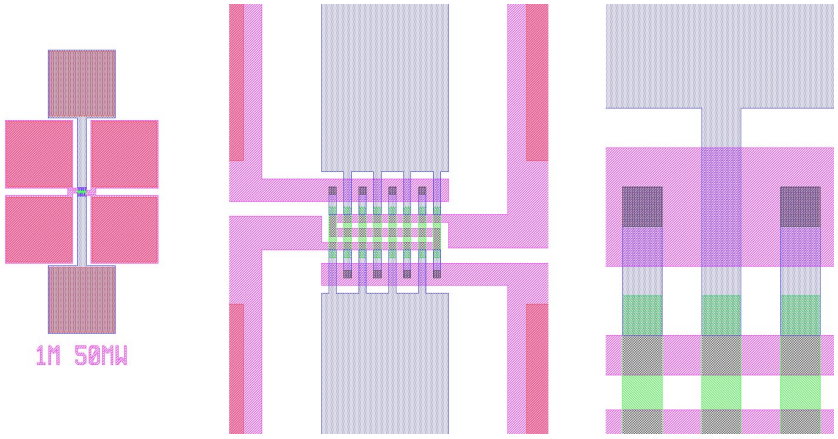

Figure 6.6 Mask design for one of the VCR designs.

The maximum wafer size compatible with the PLD chamber used to deposit the VO_2 film was 2 in, so the masks where designed for 2 in diameter wafers. the final masks also included other devices that where compatible with the process. The final full wafer mask is shown in **Figure** 6.7.

6.4 Fabrication Process Flow

The process starts with a 2 in diameter silicon wafer, 250 μm thickness. A 2 μm layer of SiO_2 is deposited by PECVD. This will isolate the metal layer from the silicon substrate. The first metal layer of 150 nm platinum with an adhesion layer of Titanium (50 nm) is deposited using liftoff (**Figure** 6.8a). A second layer of SiO_2 (only 200 nm this time)is deposited using PECVD. A layer of VO_2 is then deposited using PLD at 550 ^oC in an oxygen atmosphere. The VO_2 layer is then patterned by plasma etching (**Figure** 6.8b). Vias to the first metal

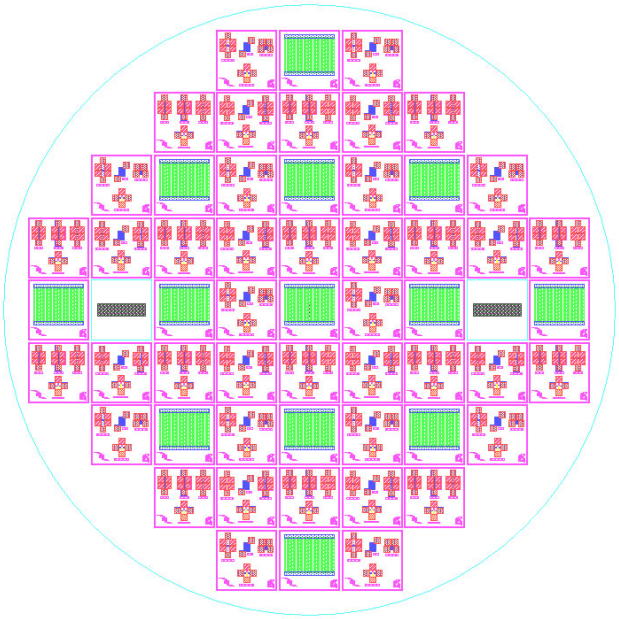

Figure 6.7 Full wafer Mask used in the VCR process.

layer are then etched using wet etching in BOE[1:5] (**Figure** 6.8c). The second metal layer is then deposited by lift-off using the same conditions as the first metal layer (**Figure** 6.8d). Another 200nm oxide layer is deposited using PECVD. Openings to the contact pads are etched using BOE[5:1]. Finally a layer of Au:Ti 150nm:50nm is deposited over the contact pads to facilitate wire bonding to the IC package (**Figure** 6.8e). The wafer is then diced (**Figure** 6.8g).

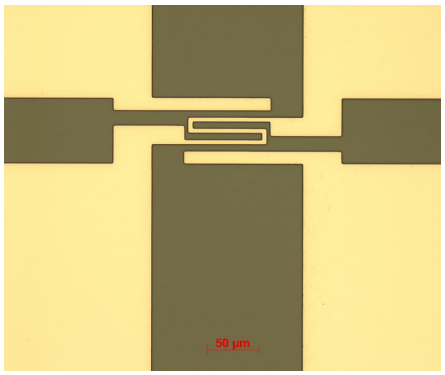

(a) After 1st metal layer.

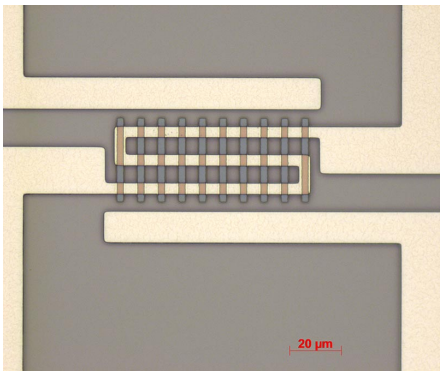

(b) After VO_2 patterning.

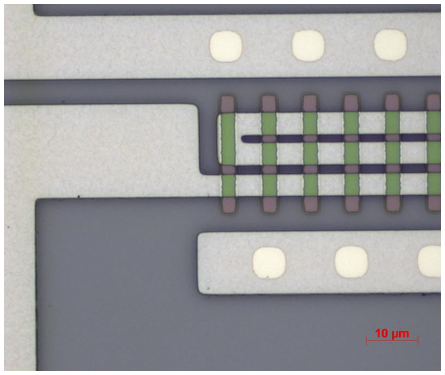

(c) After Etching vias.

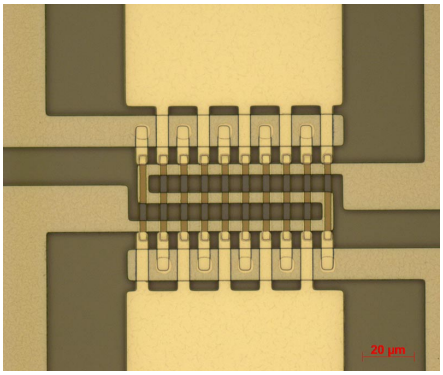

(d) After 2nd metal layer.

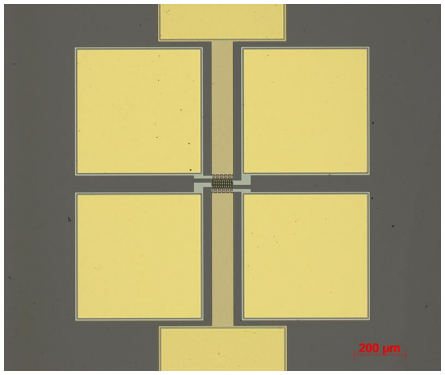

(e) After gold deposition.

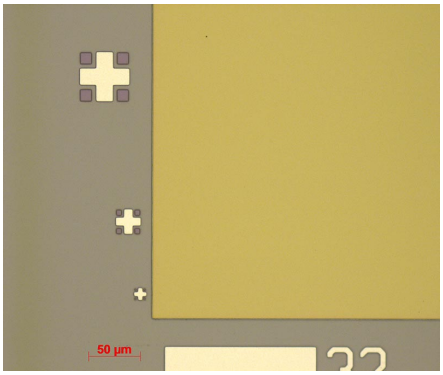

(f) Alignment marks.

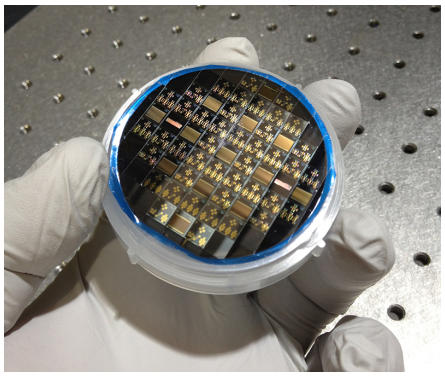

(g) Final diced wafer.

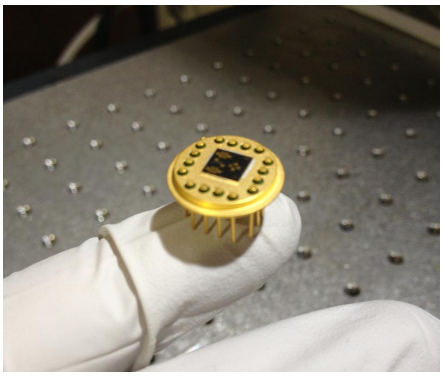

(h) DIE in IC package.

Figure 6.8 Fabrication Results.

6.5 Results

As soon as the VO_2 film was deposited, its resistance was measured as a function of temperature. the result is shown in **Figure** 6.9. These measurements were taken 1 in from the center of the substrate. These results show a good quality VO_2 film over the PECVD SiO_2 film.

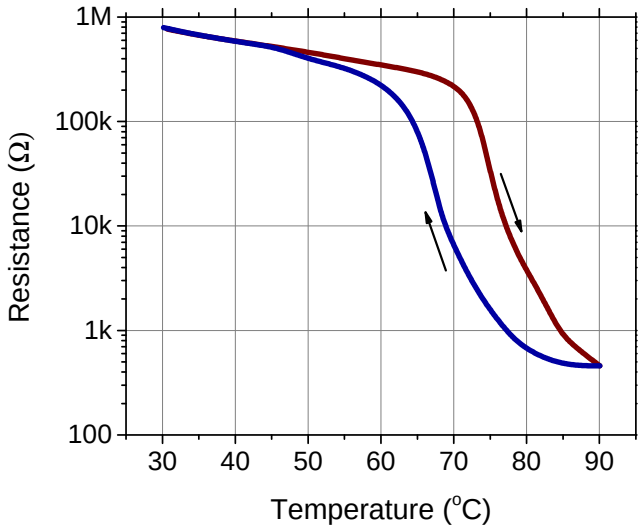

Figure 6.9 Resistance as a function of temperature for the VO_2 film right after deposition.

After device completion, several of the VCR devices were tested without the feedback circuit (in open loop). The heater voltage was slowly ramped up and down. Both VO_2 resistors where simultaneously measured, as well as the power to the heater. The results for one of these devices (200k, 200mV) are shown in **Figure** 6.10.

This shows that the minimum resistance was obtained at around the expected power of 200mW. However the total resistance drop was less that the resistance drop observed in **Figure** 6.9. There can be many causes for this drop and further experimentation is required. One possibility is that the deposition temperature of the PCVD Oxide (300 ^oC) is sufficient for causing a small change in the oxidation of the VO_2 film. There was also a difference in the resistance values of the VO_2 resistors. This difference was found to be attributed to bad adhesion between the metal contacts and the individual VO_2 strips. In some cases the

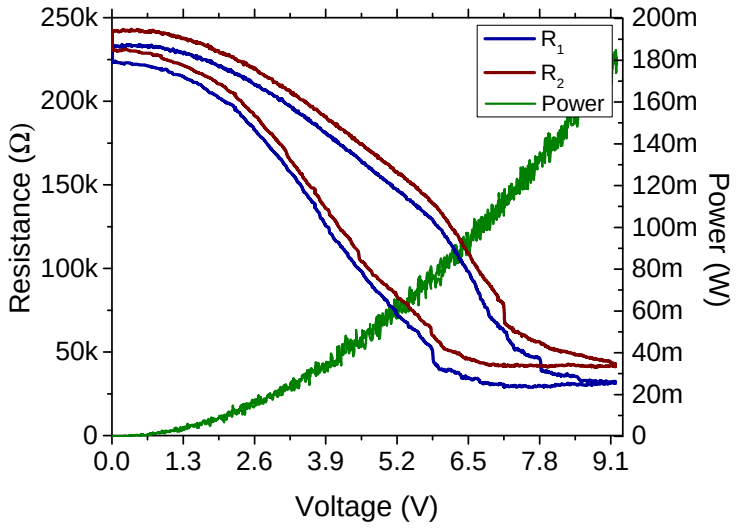

Figure 6.10 Open loop test on the 200mw 200k VCR.

metal would peal off these strips, essentially disconnecting that strip from the total resistor, changing its equivalent resistance. An example of this problem can be seen in **Figure** 6.11.

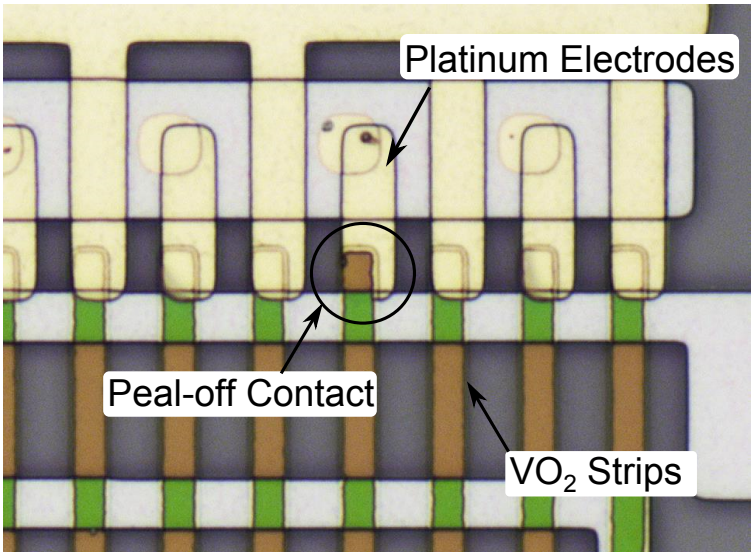

Figure 6.11 Exampe of the metal pealing off the VO_2 film.

Small resistance devices contained many of these strips forming the VO_2 resistors. So when one or two got disconnected, the total resistance was not affected too much. However larger resistance devices were composed of very few of these strips. So a few failed strips would change the resistance significantly. As an example, **Figure** 6.12 shows the open

loop response of a (500k,100mW) device, which is much smaller. In this case the difference between R_1 and R_2 is to large to efficiently use feedback compensation. This problem however does not affect the thermal properties of the device, or the transient response. Future implementations could compensate for this problem by making lower resistance devices or by maybe using adhesion promoters.

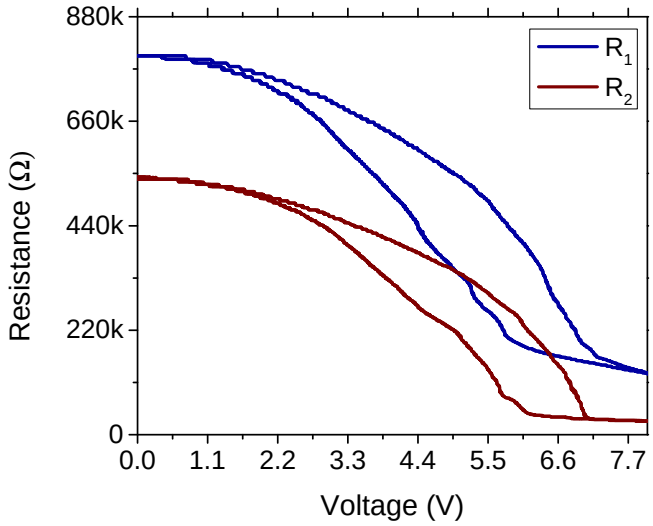

Figure 6.12 Open loop test on the 100mw 500k VCR, showing large differences in R1 and R2.

Another important parameter of the final VCR device is the response time. This is defined as how fast the value of the resistance can be changed. In order to measure this, both resistors were connected as voltage dividers and the output voltages were measured as a step input voltage was given to the heater. The results for the 200k device are shown in **Figure** 6.13. Due to the large thermal conduction between the resistor and the substrate, the time constant of the device is much faster than those reported in the previous chapters. As expected there is a difference between the heating and cooling time constants. Since the heating transient is limited by how "fast" heat can be delivered to the device and is therefore limited by the input power, the heating transient can be adjusted by changing the heater power input. However the cooling transient is limited by power dissipation through

the substrate which is fixed by the geometry of the device. **Figure** 6.14 Shows the difference in heating and cooling time constant for a (500k, 100mW) device.

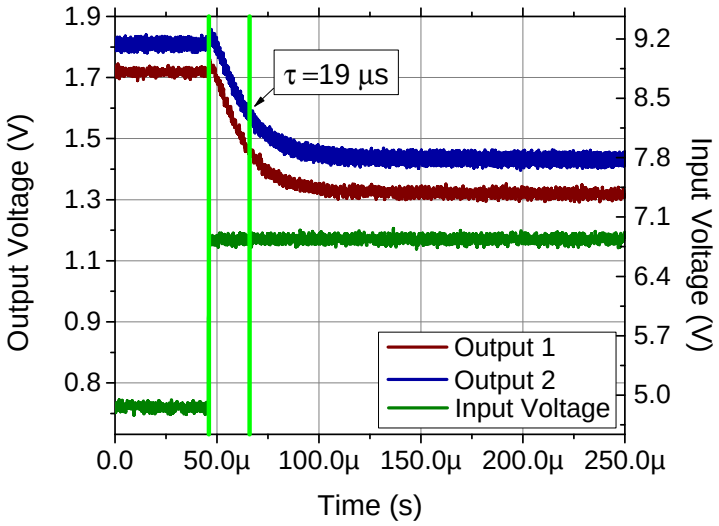

Figure 6.13 Transient response of the resistance of the VCR, due to a step input.

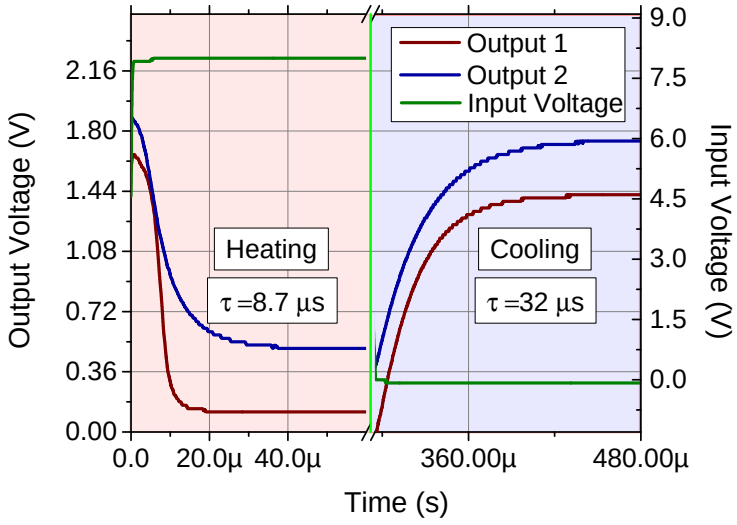

Figure 6.14 Transient response of the resistance of the 500k 100mw VCR, due to a step input for the heating and cooling cycle.

Finally, in order to test the closed loop performance the feedback circuit shown in **Figure** 6.3 was implemented using an FPGA in order to quickly tune the feedback gains. The results

shown in **Figure** 6.15 show the controlled resistance as the control voltage is varied. These results show a fairly linear response as desired.

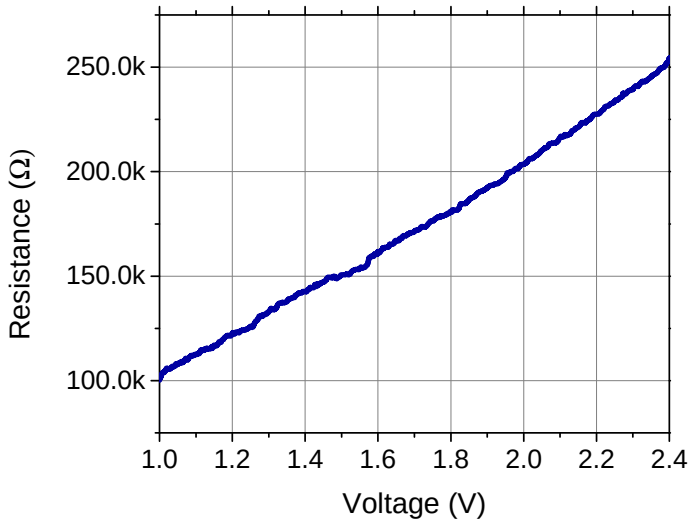

Figure 6.15 Close Loop Test on the 200 mW, 200k VCR.

6.6 Summary

This chapter presented a case study on the design of a VO_2-based device which included deposition and patterning of the VO_2 film and incorporation of the VO_2 film into the rest of the micro-fabrication process. The resulting device was measured and its open-loop and close-loop response was characterized. The complications of including VO_2 films into micro-fabrication processes were explored, and a successful VO_2 compatible fabrication process was developed. These results show that with proper workarounds, it is possible to include VO_2 in more complicated designs, greatly expanding its potential applications.

CHAPTER 7

SUMMARY

7.1 Summary of Contributions

This dissertation presented a series of studies which explored the use of the structural phase transition of VO_2 in MEMS actuators. MEMS actuators enable the interaction of devices with their surroundings, instead of simply sensing it. Actuation mechanisms, which are very common in the macro size domain, such as pneumatics, induction motors, and combustion engines, are very difficult and inefficient to implement in the micro domain. Therefore, new actuation techniques must be developed and optimized. Current actuation mechanisms such as electrostatic or thermal expansion have limited performance in terms of total displacement, applied force, operating voltage, and power requirements. This has resulted in a push to incorporate new multifunctional smart materials into standard MEMS devices to improve performance. VO_2 has proven to be one of the most promising materials for the creation of new sensors and actuators. Although most of its electrical and optical properties have been thoroughly studied, there is very little work related to its SPT and its application to MEMS actuators. Throughout this dissertation the SPT of VO_2 is extensively studied, methods are developed for the optimal design of VO_2-based actuators. The memory effect caused by the hysteresis in the SPT is exploited to create very robust programmable multiple state actuators. And fabrication processes are developed which combine the use of VO_2 with standard MEMS fabrication processes.

7.2 List of Problems Solved in this Thesis

The following are the key points addressed in this dissertation:

1. Characterization of the temperature dependent bending caused by the SPT of VO_2 in

bimorph cantilevers.

2. Characterization of the memory type behavior due to the hysteresis of the SPT in VO_2-based actuators.

3. Optimization of the design of VO_2-based bimorph actuators with embedded electric micro-heaters in terms of maximum deflection and power consumption.

4. Development of mathematical models which facilitate the future design and simulation of new VO_2-based devices.

5. Characterization of the dynamic response of VO_2-based actuators.

6. Development of a robust feedback control system which accurately controls the programed states of VO_2-actuators employing the memory effect of the SPT.

7. Development a fabrication process which permits the inclusion of VO_2 thin films in the fabrication of new MEMS devices.

BIBLIOGRAPHY

BIBLIOGRAPHY

[1] M. S. Baker and A. D. Corwin, "Design and reliability of a MEMS thermal rotary actuator.," *Sandias National Lab SAND2007-5901C*, Sept. 2007.

[2] M. C. LeMieux, M. E. McConney, Y.-H. Lin, S. Singamaneni, H. Jiang, Bunning, and V. V. Tsukruk, "Polymeric Nanolayers as Actuators for Ultrasensitive Thermal Bimorphs," *Nano Letters*, vol. 6, pp. 730–734, Mar. 2006.

[3] D. Zakharov, G. Lebedev, A. Irzhak, V. Afonina, A. Mashirov, V. Kalashnikov, V. Koledov, A. Shelyakov, D. Podgorny, N. Tabachkova, and V. Shavrov, "Submicron-sized actuators based on enhanced shape memory composite material fabricated by FIB-CVD," *Smart Materials and Structures*, vol. 21, p. 052001, May 2012.

[4] P. Baum, D. S. Yang, and A. H. Zewail, "4D Visualization of Transitional Structures in Phase Transformations by Electron Diffraction," *Science*, vol. 318, pp. 788–792, Nov. 2007.

[5] A. Rúa, F. E. Fernández, and N. Sepúlveda, "Bending in VO_2-coated microcantilevers suitable for thermally activated actuators," *Journal of Applied Physics*, vol. 107, p. 074506, Jan. 2010.

[6] E. Merced, X. Tan, and N. Seplveda, "Strain energy density of vo2-based microactuators," *Sensors and Actuators A: Physical*, vol. 196, no. 0, pp. 30 – 37, 2013.

[7] H. Coy, R. Cabrera, N. Sepúlveda, and F. E. Fernández, "Optoelectronic and all-optical multiple memory states in vanadium dioxide," *Journal of Applied Physics*, vol. 108, p. 113115, Jan. 2010.

[8] R. Cabrera, E. Merced, N. Dávila, F. E. Fernández, and N. Sepúlveda, "A multiple-state micro-mechanical programmable memory," *Microelectronic Engineering*, vol. 88, pp. 3231–3234, Nov. 2011.

[9] R. Cabrera, E. Merced, and N. Sepulveda, "Performance of Electro-Thermally Driven VO_2-Based MEMS Actuators," *Journal of Microelectromechanical Systems*, pp. 1–1, Jan. 2013.

[10] R. Cabrera, E. Merced, and N. Seplveda, "A micro-electro-mechanical memory based on the structural phase transition of vo2," *physica status solidi (a)*, vol. 210, no. 9, pp. 1704–1711, 2013.

[11] F. Morin, "Oxides Which Show a Metal-to-Insulator Transition at the Neel Temperature," *Physical Review Letters*, vol. 3, pp. 34–36, July 1959.

[12] F. C. Case, "Improved VO_2 thin films for infrared switching," *Applied optics*, vol. 30, p. 4119, Jan. 1991.

[13] N. Sepúlveda, A. Rúa, R. Cabrera, and F. Fernández, "Young's modulus of VO_2 thin films as a function of temperature including insulator-to-metal transition regime," *Applied Physics Letters*, vol. 92, p. 191913, Jan. 2008.

[14] G. Stefanovich, A. Pergament, and D. Stefanovich, "Electrical switching and Mott transition in VO2," *Journal of Physics: Condensed Matter*, vol. 12, pp. 8837–8845, Oct. 2000.

[15] J. W. Arblaster, "Crystallographic Properties of Platinum," *Platinum Metals Review*, vol. 50, pp. 118–119, July 2006.

[16] J. H. Comtois, M. A. Michalicek, and C. C. Barron, "Electrothermal actuators fabricated in four-level planarized surface micromachined polycrystalline silicon," *Sensors and Actuators A: Physical*, vol. 70, pp. 23–31, Oct. 1998.

[17] L. Que and J. Park, "Bent-beam electro-thermal actuators for high force applications," *Journal of Microelectromechanical Systems*, pp. 1–6, Jan. 1999.

[18] J. Juuti, K. Kordás, R. Lonnakko, P. V. Moilanen, and S. Leppävuori, "Mechanically amplified large displacement piezoelectric actuators," *Sensors and Actuators A: Physical*, vol. 120, pp. 225–231, Apr. 2005.

[19] N. Yamada, "Erasable phase-change optical materials," *MRS Bulletin*, vol. 21, pp. 48–50, 9 1996.

[20] C. A. Volkert and M. Wuttig, "Modeling of laser pulsed heating and quenching in optical data storage media," *Journal of Applied Physics*, vol. 86, no. 4, pp. 1808–1816, 1999.

[21] D. Wamwangi, W. Njoroge, and M. Wuttig, "Crystallization kinetics of $ge_4sb_1te_5$ films," *Thin Solid Films*, vol. 408, no. 12, pp. 310 – 315, 2002.

[22] I. Friedrich, V. Weidenhof, W. Njoroge, P. Franz, and M. Wuttig, "Structural transformations of $ge_2sb_2te_5$ films studied by electrical resistance measurements," *Journal of Applied Physics*, vol. 87, no. 9, pp. 4130–4134, 2000.

[23] T. P. L. Pedersen, J. Kalb, W. K. Njoroge, D. Wamwangi, M. Wuttig, and F. Spaepen, "Mechanical stresses upon crystallization in phase change materials," *Applied Physics Letters*, vol. 79, no. 22, pp. 3597–3599, 2001.

[24] J. Kalb, Q. Guo, X. Zhang, Y. Li, and C. Sow, "Phase-change materials in optically triggered microactuators," *Journal of Microelectromechanical Systems*, pp. 1–10, Jan. 2008.

[25] P. Krulevitch, A. Lee, P. Ramsey, J. Trevino, J. Hamilton, and M. Northrup, "Thin film shape memory alloy microactuators," *Microelectromechanical Systems, Journal of*, vol. 5, no. 4, pp. 270–282, 1996.

[26] Y.-T. Cheng and D. Grummon, "Indentation in shape memory alloys," in *Micro and Nano Mechanical Testing of Materials and Devices* (F. Yang and J. C. Li, eds.), pp. 69–84, Springer US, 2008.

[27] D. Grummon, R. Gotthardt, and T. LaGrange, "Planar extrinsic biasing of thin film shape-memory mems actuators," *Materials Research Society Symposium - Proceedings*, vol. 741, pp. 287–292, 2002.

[28] W. Ni, Y.-T. Cheng, and D. S. Grummon, "Microscopic shape memory and superelastic effects under complex loading conditions," *Surface and Coatings Technology*, vol. 177178, no. 0, pp. 512 – 517, 2004. Proceedings of the 30th International Conference on Metallurgical Coatings and Thin Films.

[29] P. Krulevitch, A. Lee, and P. Ramsey, "Thin film shape memory alloy microactuators," *Journal of Microelectromechanical Systems*, pp. 1–13, Jan. 1996.

[30] P. Dernier, "Structural investigation of the metal-insulator transition in v_6o_{13}," *Materials Research Bulletin*, vol. 9, no. 7, pp. 955 – 963, 1974.

[31] J. Feinleib and W. Paul, "Semiconductor-To-Metal Transition in V_2O_3," *Physical Review*, vol. 155, pp. 841–850, Mar. 1967.

[32] V. Eyert, "The metal-insulator transitions of VO_2: A band theoretical approach," *Annalen der Physik*, vol. 11, no. 9, pp. 650–704.

[33] K. Liu, C. Cheng, Z. Cheng, K. Wang, R. Ramesh, and J. Wu, "Giant-amplitude, high-work density microactuators with phase transition activated nanolayer bimorphs," *Nano Letters*, vol. 12, no. 12, pp. 6302–6308, 2012.

[34] A. Rúa, F. E. Fernández, R. Cabrera, and N. Sepúlveda, "Young's modulus of pulsed-laser deposited V_6O_{13}thin films," *Journal of Applied Physics*, vol. 105, p. 113504, Jan. 2009.

[35] J. Cao, E. Ertekin, V. Srinivasan, W. Fan, S. Huang, H. Zheng, J. W. Yim, D. R. Khanal, D. F. Ogletree, J. C. Grossman, and J. Wu, "Strain engineering and one-dimensional organization of metal-insulator domains in single-crystal vanadium dioxide beams," *Nature Nanotechnology*, vol. 4, pp. 732–737, Sept. 2009.

[36] F. P. Incropera, A. S. Lavine, and D. P. DeWitt, *Fundamentals of Heat and Mass Transfer*. John Wiley & Sons Incorporated, 2011.

[37] D. Ramos, N. C. Microelectronics, J. Tamayo, J. Mertens, and M. Calleja, "Photothermal excitation of microcantilevers in liquids," *Journal of Applied Physics*, vol. 99, pp. 124904–124904–8, June 2006.

[38] E. Merced, R. Cabrera, H. Coy, F. E. Fernandez, and N. Sepulveda, "Frequency Tuning of VO_2 -Coated Buckled Microbridges," *Journal of Microelectromechanical Systems*, vol. 20, pp. 558–560, June 2011.

[39] R. Cabrera, P. R. Mayagüez, E. Merced, N. Sepúlveda, and F. E. Fernández, "Dynamics of photothermally driven VO_2-coated microcantilevers," *Journal of Applied Physics*, vol. 110, pp. 094510–094510–8, Nov. 2011.

[40] E. Merced, R. Cabrera, N. Dávila, F. E. Fernández, and N. Sepúlveda, "A micromechanical resonator with programmable frequency capability," *Smart Materials and Structures*, vol. 21, p. 035007, Mar. 2012.